NAVAL POSTGRADUATE SCHOOL
Monterey, California

THESIS

A DAY IN THE LIFE OF A WARM FRONT

by

Susan A. Davies

December 1989

Thesis Advisor Wendell A. Nuss

Unclassified

security classification of this page

REPORT DOCUMENTATION PAGE

1a Report Security Classification: Unclassified		1b Restrictive Markings	
2a Security Classification Authority		3 Distribution Availability of Report: Approved for public release; distribution is unlimited.	
2b Declassification/Downgrading Schedule			
4 Performing Organization Report Number(s)		5 Monitoring Organization Report Number(s)	
6a Name of Performing Organization: Naval Postgraduate School	6b Office Symbol (if applicable): 35	7a Name of Monitoring Organization: Naval Postgraduate School	
6c Address (city, state, and ZIP code): Monterey, CA 93943-5000		7b Address (city, state, and ZIP code): Monterey, CA 93943-5000	
8a Name of Funding Sponsoring Organization	8b Office Symbol (if applicable)	9 Procurement Instrument Identification Number	
8c Address (city, state, and ZIP code)		10 Source of Funding Numbers	
		Program Element No. / Project No. / Task No. / Work Unit Accession No.	

11 Title (include security classification): A DAY IN THE LIFE OF A WARM FRONT

12 Personal Author(s): Susan A. Davies

13a Type of Report: Master's Thesis	13b Time Covered: From To	14 Date of Report (year, month, day): December 1989	15 Page Count: 81

16 Supplementary Notation: The views expressed in this thesis are those of the author and do not reflect the official policy or position of the Department of Defense or the U.S. Government.

17 Cosati Codes			18 Subject Terms (continue on reverse if necessary and identify by block number)
Field	Group	Sub-group	Warm front secondary circulation, influence of surface fluxes

19 Abstract (continue on reverse if necessary and identify by block number)

Three numerical model simulations of cyclogenesis are compared to examine the role of boundary layer stratification in enhancing the components forcing the ageostrophic circulation of an idealized warm front. The Sawyer-Eliassen diagnostic equation is applied to examine the contributions of frictional forcing and diabatic heating, as well as confluent and shear geostrophic deformation, to forcing of the secondary circulation of a warm front. The surface heat and moisture flux distributions are varied in each case, in order to evaluate the effect on each component as well as the cyclogenesis.

Results confirm previous studies that geostrophic deformation forces strong frontogenesis at the surface, and at mid-levels frontogenesis is weaker and forced primarily by latent heat release. Frontogenetical forcing is modified by small-scale frictional forcing and diabatic heating, which depend upon the surface and boundary layer processes. Although frictional forcing comprises less than five percent of total forcing of the warm front, it apparently enhances frontogenesis, partially due to indirect effects on other more dominant processes. The intensity of frictional forcing is strongly dependent on the surface heat flux distribution and track of the cyclone relative to the sea-surface temperature gradient. In the absence of surface fluxes, frictional forcing is negligible. Surface forcing due to diabatic heating is frontolytical, and reduces total forcing at low levels by about twenty percent. The magnitude of the frontolytical forcing by diabatic heating at low levels is only partially dependent on the surface heat and moisture flux distribution. Even in the absence of surface heat and moisture fluxes, the frontolytical forcing persisted, suggesting problems with the cumulus parameterization or errors in the computation of this term. These results remain to be verified against an actual case study of a warm front.

21 Distribution/Availability of Abstract	21 Abstract Security Classification	
☒ unclassified/unlimited ☐ same as report ☐ DTIC users	Unclassified	
22a Name of Responsible Individual: Wendell A. Nuss	22b Telephone (include Area code): (408) 646-3275	22c Office Symbol: 63NU

DD FORM 1473,84 MAR — 83 APR edition may be used until exhausted; All other editions are obsolete — security classification of this page

Unclassified

Approved for public release; distribution is unlimited.

A Day in the Life of a Warm Front

by

Susan A. Davies
Lieutenant Commander, United States Navy
B.A., University of California, San Diego, 1980

Submitted in partial fulfillment of the
requirements for the degree of

MASTER OF SCIENCE IN METEOROLOGY AND PHYSICAL OCEANOGRAPHY

from the

NAVAL POSTGRADUATE SCHOOL
December 1989

ABSTRACT

Three numerical model simulations of cyclogenesis are compared to examine the role of boundary layer stratification in enhancing the components forcing the ageostrophic circulation of an idealized warm front. The Sawyer-Eliassen diagnostic equation is applied to examine the contributions of frictional forcing and diabatic heating, as well as confluent and shear geostrophic deformation, to forcing of the secondary circulation of a warm front. The surface heat and moisture flux distributions are varied in each case, in order to evaluate the effect on each component as well as the cyclogenesis.

Results confirm previous studies that geostrophic deformation forces strong frontogenesis at the surface, and at mid-levels frontogenesis is weaker and forced primarily by latent heat release. Frontogenetical forcing is modified by small-scale frictional forcing and diabatic heating, which depend upon the surface and boundary layer processes. Although frictional forcing comprises less than five percent of total forcing of the warm front, it apparently enhances frontogenesis, partially due to indirect effects on other more dominant processes. The intensity of frictional forcing is strongly dependent on the surface heat flux distribution and track of the cyclone relative to the sea-surface temperature gradient. In the absence of surface fluxes, frictional forcing is negligible. Surface forcing due to diabatic heating is frontolytical, and reduces total forcing at low levels by about twenty percent. The magnitude of the frontolytical forcing by diabatic heating at low levels is only partially dependent on the surface heat and moisture flux distribution. Even in the absence of surface heat and moisture fluxes, the frontolytical forcing persisted, suggesting problems with the cumulus parameterization or errors in the computation of this term. These results remain to be verified against an actual case study of a warm front.

TABLE OF CONTENTS

LIST OF FIGURES

ACKNOWLEDGEMENT

My thanks to Professor Wendell Nuss for his patience with an aviator.

I. INTRODUCTION

A. CYCLOGENESIS AND FRONTOGENESIS

Mid-latitude cyclones are transient waves in the global zonal flow that perform an important role in transporting heat and momentum in the atmosphere. Historically, cyclone development was explained as a wave instability on the polar front, with the existence of the front considered a necessary precursor for cyclogenesis. This theory, known as the polar front theory of cyclogenesis, significantly influenced Petterssen (1956) who related cyclogenesis to the interaction of vorticity advection aloft with surface frontal features. The modern view, based on baroclinic instability theory, considers fronts to be a consequence of the development of a cyclone and a source of baroclinic energy for cyclogenesis. The baroclinicity of the atmosphere and the synoptic-scale flow combine to lead to cyclogenesis, the development of sub-synoptic scale fronts, and the formation of jet streaks.

The basic premise of baroclinic instability theory is that the circulation of a cyclone results from any small perturbation forced by advection of positive (cyclonic) vorticity aloft with the advance of the upper-level wave or by warm advection at low levels over a broad region. Geostrophic deformation associated with cyclogenesis acts to enhance the temperature gradient in particular regions of a cyclone. This process is known as frontogenesis. Vertical and divergent ageostrophic motions arise in response to frontogenesis, and are the mechanism for the adjustment of vorticity and thermal properties to return the system to thermal wind balance. The ageostrophic circulations associated with frontogenesis are small-scale manifestations of the basic synoptic-scale forcing. Although these synoptic-scale processes are thought to be the primary processes for cyclogenesis, frontogenesis is a secondary process that may feed back on the synoptic-scale forcing to produce stronger cyclogenesis than that given by just the synoptic-scale forcing. The interaction between synoptic-scale vorticity and temperature advection and mesoscale frontogenesis in cyclones is not yet completely understood.

1. Sub-Synoptic Scale Processes

Recent cyclogenesis studies suggest important coupling between cyclogenesis and mesoscale processes associated with frontogenesis and jet streaks. Uccellini et al. (1985, 1987) and Keyser and Shapiro (1986) have shown that small scale upper-level baroclinic processes associated with upper-level jet streaks enhance the vertical circu-

lation and cyclogenesis. Strong jet streak divergence induces a secondary circulation that extends through the depth of the troposphere. This enhances the development of a low-level jet and cyclogenesis at the surface. This mesoscale process is considered to be an important mechanism for some explosive cyclones.

Another important mechanism in some explosive cyclones is the release of latent heat in the mid-troposphere. The release of latent heat also influences the frontogenesis process. Williams et al. (1981), using a numerical model, and Thorpe (1984), using an analytical quasi-geostrophic model, showed that latent heat release on the warm side of the front is frontogenetical aloft. The heating directly increases the temperature gradient at levels of large heating, and the induced divergent circulation leads to convergence below the heating which increases the temperature gradient in that region. The precipitation maximum occurs where the vertical motion is a maximum. Evaporative cooling occurs when precipitation falls through dry air below on the cold side of fronts, thus enhancing the cross-front temperature gradient ahead of the front.

2. Planetary Boundary Layer Processes

Although baroclinic synoptic and mesoscale processes mentioned above are dominant, the importance of surface and boundary layer processes also has been demonstrated in recent studies. The boundary layer processes contribute to cyclogenesis and frontogenesis through thermodynamic effects due to the heat and moisture fluxes, and dynamic effects due to friction. Friction further disrupts geostrophic balance and increases the ageostrophic component of the wind through frictional wind turning. This results in an additional component of convergence and shear due to friction. Keyser and Anthes (1982) showed that convergence due to surface friction acts frontogenetically at the surface. Behind the frontal zone the vertical shear of the ageostrophic wind, which is frictionally induced, acts to diminish the static stability in the planetary boundary layer (PBL) and enhance the static stability at the top of the boundary layer. Ahead of the front, differential temperature advection by the ageostrophic component of the wind acts to increase the static stability in the boundary layer and decrease the static stability at the top of the boundary layer. The result is a compressed thermal gradient in the PBL, which is frontogenetical. Keyser and Anthes (1982) also showed that frictional convergence drives a vertical velocity jet above the surface front. This vertical jet is a component of the secondary circulation.

Danard and Ellenton (1980) evaluated the surface heating in several east coast U. S. cyclones, and concluded that the surface heating acted to decrease the low-level baroclinicity by warming the cold advection regions and vice versa. This finding is

consistent with previous studies of the effects of surface heating in baroclinic instability models, and indicates a frontolytical role of the surface heat flux. However, in studies of the Presidents' Day storm of 1979, Bosart (1981) and Bosart and Lin (1984) indicated that the low-level contributions by the surface heat and moisture fluxes were important to cyclogenesis. They found that positive heat fluxes to the northeast of the surface low potentially contributed to rapid development through distribution of the cyclogenetic environment. Reed and Albright (1986) found similar results in their study of an eastern North Pacific cyclone.

A favorable surface heat and moisture flux distribution can also enhance frontogenesis and cyclogenesis through the associated latent heat release above the boundary layer. Chen et al. (1983) found that mid-tropospheric latent heating decreased when the surface heat and moisture fluxes were removed. Atlas (1987) found that the vertical transport of air that is heated and moistened by the surface heat and moisture fluxes can result in significant mid-tropospheric heating through the release of latent heat.

B. MARINE CYCLONES

Compared with continental and coastal cyclones, marine cyclones have a more complex surface heat and moisture flux distribution contributing to frontogenesis and cyclogenesis, due to the influence of the sea-surface temperature (SST) distribution. Businger and Shaw (1984) suggested that for a simple uniform flow across an SST gradient, PBL convergence will result from stratification effects on the frictional wind turning as the wind flows across an SST gradient. As a cyclone moves across a fixed SST distribution, changes in the frictional convergence and the transport of boundary layer air to the mid-troposphere are likely to occur. In their study of surface fluxes and divergence in Storm Transfer and Response Experiment (STREX) storms, Fleagle and Nuss (1985) showed that the distributions of the frictional convergence and vertical velocity at the top of the PBL are primarily determined by the horizontal distribution of the surface wind stress. In turn, the wind stress depends not only on the synoptic-scale forcing at the top of the PBL, but also on the PBL stratification, the surface heat flux distribution, and thermal wind turning in the PBL. Nuss (1989) showed that stable stratification behind the warm front, and unstable stratification ahead of the warm front in a region of upward heat fluxes, apparently resulted in enhanced frictional convergence ahead of the front. Danard (1986) found that increasing the SST by five degrees resulted

in greater boundary layer convergence and enhanced convective heating in the model cyclogenesis.

Nuss and Anthes (1987) studied the effect of surface fluxes and boundary layer influences on an idealized marine cyclone. They showed that although baroclinic instability, which depends on the vertical wind shear and static stability, as shown originally by Charney (1947) and Eady (1949), is sufficient for rapid cyclogenesis, relatively small changes in the low-level static stability, meridional temperature gradient, and surface heat and moisture fluxes significantly modified the development of the model cyclone. These low-level changes resulted entirely from varying the SST distribution. They found that the deepening rate of the cyclone increased by 25% for complete removal of the surface heat and moisture fluxes, and increased by 15% for a modified SST distribution in phase with the low-level temperature pattern.

These results were further analyzed by Nuss (1989), in order to clarify the role of surface fluxes in the overall development of the cyclone. He found that the effect of surface heat and moisture fluxes on the structure and dynamics of oceanic cyclones can be substantial and that strictly boundary layer processes act to enhance the vertical circulation and cyclogenesis through a dynamic feedback process. Specifically, he found that the effect of surface heat and moisture fluxes depends critically on their distribution relative to the cyclone. For a zonal SST distribution, patterns of surface heating counteract PBL temperature advection and oppose cyclogenesis, as found in previous studies, including Danard and Ellenton (1980). For a sinusoidal SST distribution essentially in phase with the low-level temperature distribution, the resultant pattern of surface heating yielded unstable stratification to the northeast and stable stratification south of the warm front. This acted to enhance cyclogenesis through enhanced frictional convergence as well as increased heat and moisture transport to the surface cyclone from the northeast.

The relationship of enhanced frictional convergence to other frontogenesis processes was not examined and is the focus of this study. Although the surface heating pattern may be a damping effect, associated mid-tropospheric latent heat release increases the temperature gradient and cyclogenesis, which indirectly enhances the PBL frontogenesis processes. This indirect relationship between surface diabatic processes and the intensity of the geostrophic frontogenesis and cyclogenesis is not well understood. Uccellini et al. (1987) have demonstrated the importance of the non-linear coupling between boundary layer processes, latent heat release, and jet stream forcing along a coastal front for the Presidents' Day storm. For open ocean cyclones, the warm front region is likely

to be the focal point of the interaction between surface fluxes, diabatic heating, and the jet, as suggested by Nuss (1989), and will be the subject of this study. Studies by Emanuel (1985, 1988) and Sanders (1986) also suggest that latent heat processes associated with the warm front may contribute to enhanced cyclogenesis over the ocean.

C. OBJECTIVE

The purpose of this research is to quantify the contributions of various forcing mechanisms to the secondary circulation around a warm front, and assess their impact on the development of a cyclone. The influence of the surface heat and moisture fluxes on the frictional forcing and diabatic heating, and resultant secondary circulation, is of particular interest since it is not as clearly understood as the larger-scale geostrophic deformation processes. In addition, the feedback of these diabatic processes on the geostrophic deformation and warm frontal intensification will be examined. The specific objectives are:

1. Diagnose the geostrophic versus diabatic processes in warm frontogenesis to distinguish frictional convergence from pure geostrophic deformation;

2. Describe the feedback mechanism of surface heat fluxes on geostrophic and diabatic forcing by quantifying their frontogenetic effects on the friction and latent heat release and their frontolytical effects on the PBL thermal gradient;

3. Describe the time evolution of the forcing;

4. Obtain an understanding of the interaction of the SST with fronts.

The Sawyer-Eliassen diagnostic equation will be used to diagnose the forcing of the vertical circulation around the warm front in three numerical simulations of cyclogenesis. The Sawyer-Eliassen equation is reviewed in Section II, followed by a brief description of the model experiments in Section III. Section IV compares the results of the three simulations. A discussion of these results is given in Section V, followed by conclusions and recommendations for future research in Sections VI and VII.

II. BACKGROUND

Sawyer (1956) showed how the secondary circulation around fronts can be calculated on the basis of quasi-geostrophic theory, and Eliassen (1959, 1962) extended his work to include friction and latent heating effects, as well as the vertical shear in the cross-front plane, to the forcing of the secondary circulation. They developed the theory of describing temporal changes in the vertical and horizontal gradients of temperature and absolute momentum in the cross-front plane in terms of the induced geostrophic and ageostrophic deformation field. It is from this theory that the Sawyer-Eliassen diagnostic equation for the secondary circulation was derived. This equation enables diagnosis of small-scale diabatic and frictional processes as well as those processes associated with geostrophic deformation forcing the secondary circulation around a front. Eliassen (1962) demonstrated that the circulation is counter-clockwise (cyclonic) around regions of positive forcing, and clockwise (anti-cyclonic) around regions of negative forcing. The circulations are concentric ellipses in the vicinity of the point source of forcing (Fig. 1), oriented vertically along the front and becoming vertically or horizontally distorted at some distance from the point source as a function of vorticity and inertial stability (Keyser and Shapiro 1986). The Sawyer-Eliassen equation was later expanded by Hoskins and Draghici (1977) and Hoskins et al. (1978) to account for variations in the along-front plane, thus generalizing the theory of secondary circulation into three dimensions, known as the Q-vector theory. The resultant equation is known as the three-dimensional (3-D) form of the Sawyer-Eliassen equation.

A. AGEOSTROPHIC CIRCULATION AROUND A WARM FRONT

Gidel (1978) describes the processes of geostrophic balance and continuity of mass flow which lead to the secondary circulation around a warm front. The rising motion within the front coupled with the sinking motion on the cold air side of the front is a thermodynamically direct circulation. By continuity of mass, the flow is convergent at low levels in the upward vertical motion region and divergent at upper levels. Transverse flow results at lower and upper levels, completing the circulation cell in the region. Upper-level westerly (positive) momentum and low level easterly (negative) momentum are created, which contribute to increasing the vertical shear of the along-front wind component. The adiabatic cooling of the rising warm air and adiabatic warming of the sinking cold air contribute to decreasing the temperature gradient across the front. Figs.

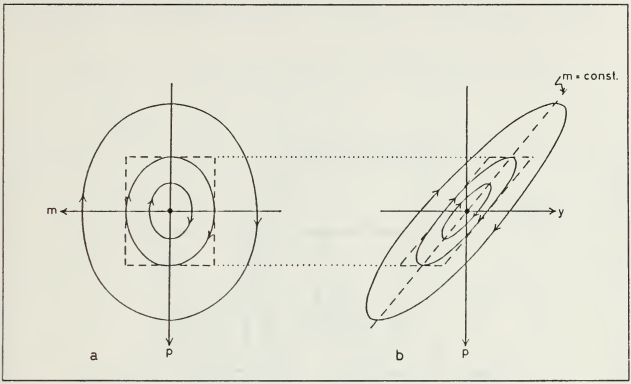

Fig. 1. Streamlines around a positive point source. Streamlines in the (a) mp-plane and in the (b) yp-plane. m denotes absolute momentum. From Eliassen (1962).

2 and 3, from Gidel (1978), depict the initial and advected potential temperature surfaces and isotachs, and the induced secondary circulation around a warm front. In the frontal zone the wind field is stronger than that required for geostrophic balance, implying that Coriolis dominates the PGF, which sets up a transverse flow to the right (north). Immediately ahead of the front, the opposite is true, and the resultant transverse flow is to the left (south). The flow is convergent directly beneath the front, and divergent behind and ahead of the front. The convergence near the leading edge of the frontal zone acts as a deformation field which enhances the potential temperature gradient across the front. The circulation cell behind the front is thermodynamically indirect and is the indirect cell discussed by Eliassen (1962) with respect to warm fronts. In the indirect circulation, the cross-front thermal gradient is enhanced by adiabatic processes and the along-front vertical wind shear is diminished by low-level divergence and upper-level convergence.

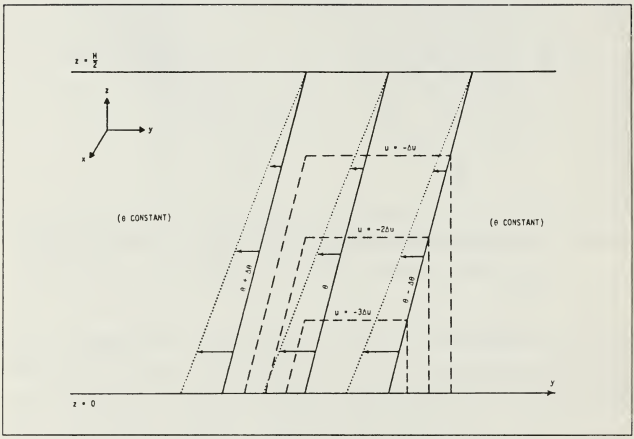

Fig. 2. Idealized cross section through a warm front. The initial position of the potential temperature surfaces is indicated by the solid lines, and their position after they have been slightly advected is indicated by dotted lines. The dashed lines are isotachs of the along-front wind field in geostrophic balance with the initial potential temperature field. From Gidel (1978).

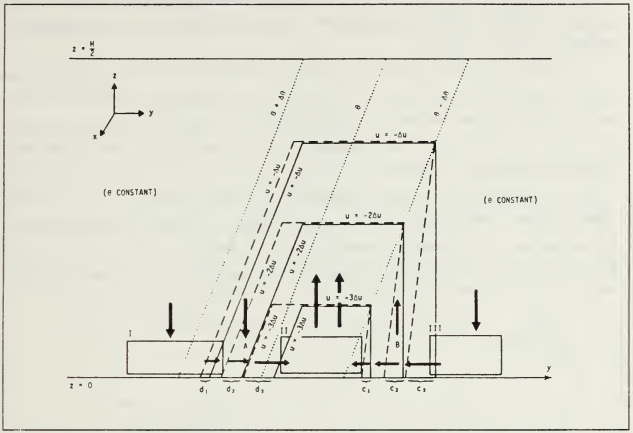

Fig. 3. Secondary circulation around a warm front. The dotted lines are repeated from Fig. 2. The dashed lines are the isotachs of the along-front wind field after being advected from their initial position shown in Fig. 2. The solid lines are the isotachs of the along-front wind field u which geostrophically balances the potential temperature field, shown as dotted lines. The heavy arrows indicate horizontal and vertical components of the induced circulation. From Gidel (1978).

The ageostrophic flow around a positive center of forcing is counter-clockwise, which gives the sense of the secondary direct circulation cell if it was located ahead of the warm front. Similarly, a negative (clockwise) center gives the direction of flow of the indirect cell if the center was located behind the front. Fig. 4a is a depiction of the theoretical location of the positive and negative ellipses of forcing around a warm front. A dipole effect is set up between the two centers, and the gradient of forcing from one cell to the other is depicted as strongest across the vertical flow regions, assuming the downward and upward motions are the same magnitude. Theoretically, the stronger the

magnitude and gradient of the cells, the stronger the magnitude of flow of the circulation cell. If the updraft region is stronger than the downdraft region, one would expect the gradients to be as in Fig. 4b.

The above discussion assumes the scale of geostrophic and diabatic forcing is the same as that of the circulation cell. However, processes which contribute to enhancement of the circulation cell are not on the same scale. The Sawyer-Eliassen equation is a means by which the small-scale processes of friction and diabatic heating can be included with geostrophic deformation to diagnose the forcing of the cell. Total forcing would not necessarily be a single symmetric center, but rather a center distorted by smaller regions of positive and negative forcing acting to enhance or retard the secondary circulation. For example, one would expect enhanced regions of forcing at low levels due to geostrophic and frictional confluence, and at mid-levels due to latent heat release.

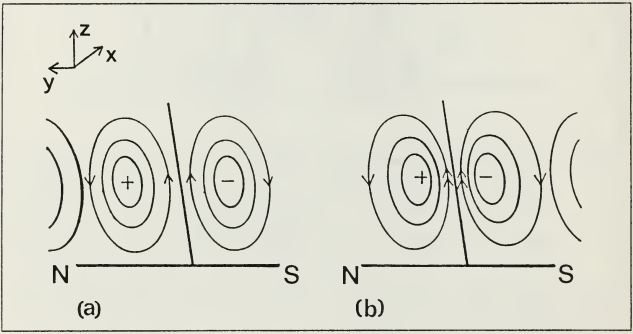

Fig. 4. **Ageostrophic forcing centers around a warm front.** Ellipses of forcing are for (a) an updraft and downdraft of equal strength, and (b) a stronger updraft. Note the orientation of the front and x- and y-axes have been reversed from Figs. 2 and 3.

B. SAWYER-ELIASSEN EQUATION

Eliassen (1962) introduced the quantity *absolute momentum* to describe the secondary circulation in terms of an absolute frame of reference, the equations for which can be written as

$$m_x = u_g - fy \tag{1}$$

and

$$m_y = v_g + fx \tag{2}$$

The thermal wind relationships in pressure coordinates are

$$\frac{\partial u_g}{\partial p} = -\frac{\partial \theta}{\partial y} \tag{3}$$

and

$$\frac{\partial v_g}{\partial p} = -\frac{\partial \theta}{\partial x} \tag{4}$$

Following Hoskins and Draghici (1977), and Keyser and Shapiro (1986), prognostic equations for absolute momentum and thermal advection can be written as

$$\frac{d}{dt}\left(\frac{\partial m_x}{\partial p}\right)_i = \frac{d}{dt}\left(\frac{\partial u_g}{\partial p}\right) = \left[-J_{yF}(u_g, v_g) - J_{yF}(m_x, v_{ag}) + \frac{\partial F_x}{\partial p}\right]_i, \tag{5}$$

$$\frac{d}{dt}\left(\frac{\partial m_y}{\partial p}\hat{j}\right) = \frac{d}{dt}\left(\frac{\partial v_g}{\partial p}\right) = \left[J_{xp}(u_g, v_g) + J_{xp}(m_y, v_{ag}) + \frac{\partial F_y}{\partial p}\right]\hat{j}, \tag{6}$$

$$\frac{d}{dt}\left(\gamma\frac{\partial\theta}{\partial y}\right)\hat{i} = \left[J_{yp}(u_g, v_g) + \gamma J_{yp}(\theta, \omega) + \left(\frac{\partial m_x}{\partial p}\frac{d\ln\gamma}{dp}\right)\omega + \gamma\frac{\partial\dot{Q}}{\partial y}\right]\hat{i}, \tag{7}$$

$$\frac{d}{dt}\left(-\gamma\frac{\partial\theta}{\partial x}\right)\hat{j} = \left[J_{xp}(u_g, v_g) + \gamma J_{yp}(\theta, \omega) + \left(\frac{\partial m_y}{\partial p}\frac{d\ln\gamma}{dp}\right)\omega + \gamma\frac{\partial\dot{Q}}{\partial x}\right]\hat{j}, \tag{8}$$

where $J_{ab}(c,d) = \frac{\partial a}{\partial c}\frac{\partial b}{\partial d} - \frac{\partial a}{\partial d}\frac{\partial b}{\partial c}$ is the Jacobian operator,

$\frac{d}{dt} = \frac{\partial}{\partial t} + u\frac{\partial}{\partial x} + v\frac{\partial}{\partial y} + \omega\frac{\partial}{\partial p}$,

$\omega = \frac{dp}{dt}$,

$F_x = \frac{\partial T_x}{\partial p}$, and $F_y = \frac{\partial T_y}{\partial p}$, where T is the stress on a horizontal surface,

$\dot{Q} = \frac{d\theta}{dt}$, and

$\gamma = \frac{R}{fp_0}\left(\frac{p_0}{p}\right)\exp\left(\frac{C_v}{C_p}\right)$.

By rearranging the terms, the x and y components of the Sawyer-Eliassen equation can be written as

$$\left[J_{yp}(m_x, v_{ag}) + \gamma J_{yp}(\theta, \omega) + \left(\frac{\partial m_x}{\partial p}\frac{d\ln\gamma}{dp}\right)\omega\right]\hat{i} = \left[-2J_{yp}(u_g, v_g) + \frac{\partial F_x}{\partial p} - \gamma\frac{\partial\dot{Q}}{\partial y}\right]\hat{i} \tag{9}$$

and

$$[J_{xf}(m_y, u_{ag}) + \gamma J_{xf}(\theta, \omega) + (\frac{\partial m_y}{\partial p}\frac{d\ln\gamma}{dp})\omega]\hat{j} = [-2J_{xp}(u_g, v_g) + \frac{\partial F_y}{\partial p} - \gamma\frac{\partial Q}{\partial x}]\hat{j} \qquad (10)$$

By taking the dot product of $-\hat{k} \times \gamma\nabla\theta$ and the vector equation made up of the x and y components given above, the magnitude of the forcing and circulation can be obtained. The right hand side (forcing) of the equation becomes

$$-2\gamma[(\frac{\partial\theta}{\partial x})^2\frac{\partial u}{\partial x} + (\frac{\partial\theta}{\partial y})^2\frac{\partial v}{\partial y}] - 2\gamma\frac{\partial\theta}{\partial x}\frac{\partial\theta}{\partial y}(\frac{\partial v}{\partial x} + \frac{\partial u}{\partial y}) - [\frac{\partial\theta}{\partial y}\frac{\partial F_x}{\partial p} - \frac{\partial\theta}{\partial x}\frac{\partial F_y}{\partial p}]$$

$$+ \gamma[\frac{\partial\theta}{\partial y}\frac{\partial Q}{\partial y} + \frac{\partial\theta}{\partial x}\frac{\partial Q}{\partial x}] \qquad (11)$$

The terms are then normalized by dividing by $|\hat{k} \times \gamma\nabla\theta|$, to obtain the magnitudes of the components contributing to total kinematic forcing of the warm front. The Sawyer-Eliassen equation is not solved; rather this form enables a diagnosis of the contributions to the forcing of the circulation cell by each term. Centers of positive and negative forcing are derived by this diagnosis, and represent centers of counter-clockwise and clockwise circulation respectively. The 3-D form is used in place of the 2-D version because the data set is three-dimensional and because the along-front gradients are not assumed to be in geostrophic balance.

C. DESCRIPTION OF TERMS

1. Geostrophic Confluence

The first term in equation (11) represents the effect that confluent geostrophic deformation has in enhancing the horizontal temperature gradient ($\nabla_p T$) by compressing the isotherms across the front. The strongest centers of confluence (positive forcing) and diffluence should be as in Fig. 5. The low-level confluence and upper-level diffluence represent a downward transport of momentum, which acts to reduce the vertical wind shear, while at the same time the thermal gradient is increasing. Following Keyser and Shapiro (1986), the resultant contributions to $d(\frac{\partial m}{\partial p})$ / dt and $d(\gamma\frac{\partial\theta}{\partial y})$ / dt are respectively negative and positive, which is a tendency towards imbalance in the thermal wind, a frontogenetic process. This imbalance is counteracted by the secondary direct circulation forced by the confluence, which simultaneously increases the vertical wind shear

through the net upward transport of positive momentum, while reducing the temperature gradient by adiabatic processes.

2. Geostrophic Shear

The second term represents the effect that geostrophic shear deformation has in rotating the along-front temperature gradient perpendicular to the front. If the winds across the front increase to a maximum at the low level easterly jet on the cold air side (ahead) of a warm front, cyclonic shear is present. If the easterly wind ahead of the front is stronger than that behind the front, differential cyclonic shear in the presence of along-front decreases in potential temperature tends to enhance the cross-front temperature gradient. Larger negative values of u_g ahead of the front relative to weaker values behind the front ($\frac{\partial u_g}{\partial y} < 0$) differentially advect higher values of potential temperature at a greater rate north of the front relative to south of the front. At the same time, the vertical wind shear ($\frac{\partial v}{\partial p}$) tends to tip the u_g isotachs into the vertical where the horizontal shear is cyclonic, thus reducing the magnitude of the vertical wind shear, creating an imbalance. Again, the direct circulation would counteract the imbalance created by the shear as with the confluence. One would expect that the strongest forcing due to shear would be between the low-level easterly jet and the front.

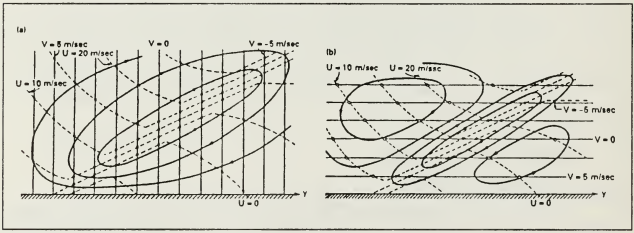

Fig. 5. Transverse ageostrophic circulations for an idealized front. Circulations characterized by (a) confluence ($\frac{\partial v_g}{\partial y} < 0, \frac{\partial v_g}{\partial p} = 0$) and (b) horizontal shear ($\frac{\partial v_g}{\partial y} = 0, \frac{\partial v_g}{\partial p} > 0$). Dashed lines, isotachs of u_g (denoted by U); thin solid lines, isotachs of v_g (denoted by V); thick solid lines, streamlines of ageostrophic circulation. Adapted from Eliassen (1962). From Keyser and Shapiro (1986).

3. Friction

The third term represents the convergent effect that friction has on the geostrophic wind. Winds at the surface experience friction, but are maintained in part by the downward momentum flux from stronger winds above the surface. Differential downward momentum fluxes act like confluence to compress the temperature gradient. As the cyclone intensifies the winds increase, which leads to increased friction and frictional turning of the winds toward the low. This enhances frictional convergence. If the winds were to increase uniformly around the low, there would be no differential momentum flux across the front. However, the wind gradient across a frontal zone is greater than elswhere around the low, so the maximum differential friction is in the vicinity of the fronts.

As discussed in Section I, favorable surface heat fluxes also enhance frictional convergence. Regions of upward heat flux into the PBL from a relatively warm surface can be likened to warm air advection into the region. This would cause a veering of the PBL wind with height, or an increased turning angle and further convergence at the surface. Similarly, a downward heat flux from the PBL to a cool surface would cause a backing of the thermal wind with height, or a reduced angle of turning and reduced convergence. For a warm front in which there are downward heat fluxes in the cold air sector ahead of the warm front as well as in the warm air sector behind the front, one can expect that for a given SST distribution, the air-sea temperature difference would be greater in the warm air region behind the front than in the cool air region ahead of the front. The downward heat flux would be greater behind the front than ahead, with the backing of the thermal wind stronger behind the front than ahead. This creates a net differential across the front, with stronger convergence ahead of the front. Thus, the frictional convergence is composed of the geostrophic component and a heat flux component. Fig. 6 depicts the geostrophic frictional forcing as a result of the differential downward transfer of momentum from the winds above the PBL, and the heat flux component of frictional forcing within the PBL due to surface heat fluxes. The depiction is for the case of stronger downward momentum fluxes behind the front than ahead, and for stronger downward heat fluxes at the surface behind the front. This would result in a reinforcement of frictional confluence. The greatest differential would be across the warm front, and the strongest frictional confluence would be located where the strongest differential occurs. Realistically it is possible to have stronger downward momentum fluxes ahead of the warm front, which would oppose the heat flux component depicted above, resulting in negligible frictional forcing.

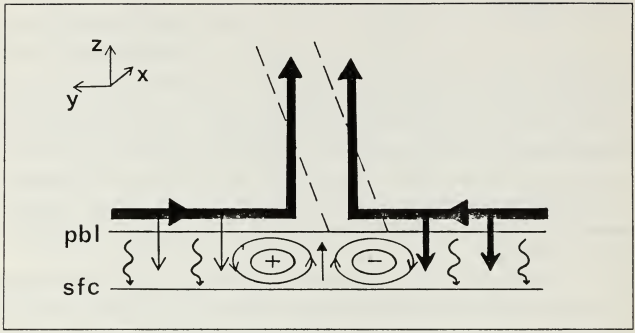

Fig. 6. Centers of frictional forcing. Heavy lines above PBL denote secondary circulation cells, with vertical arrows in the PBL denoting downward momentum fluxes (solid) and downward heat fluxes (curved). Heavy arrows indicate stronger downward momentum fluxes. Dashed lines depict warm front.

4. Diabatic Heating

The fourth term represents the effect diabatic heating has on the horizontal temperature gradient. In the boundary layer, differential heat fluxes act to relax the temperature gradient, and are strongly dependent upon the surface temperature distribution, as discussed in Section I. Surface heat and moisture fluxes in the PBL can be turbulently mixed out of the PBL, providing a source of heat and moisture to the mid-troposphere in addition to the heat and moisture advected into the region. At mid-levels, latent heat release within and behind the warm front, and evaporative cooling ahead of the front enhance the temperature gradient. One should expect centers of positive and negative diabatic forcing to be located as in Fig. 7. The low level forcing opposes the secondary circulation at low levels and the mid level forcing enhances the circulation.

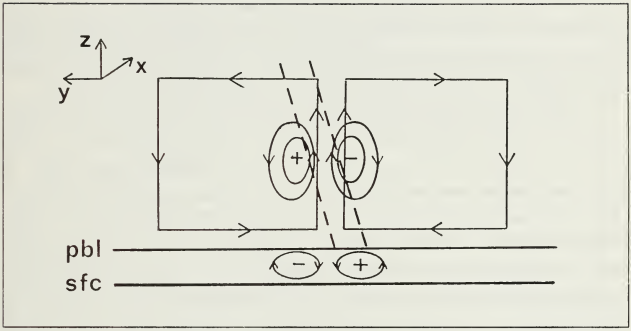

Fig. 7. **Centers of diabatic forcing.** Forcing in the PBL opposes the secondary circulation. In the mid-troposphere it enhances the circulation.

III. DESCRIPTION OF DATA SET

A. NUMERICAL MODEL

The numerical simulations for the three case studies used in this study were run for 48 hours using the Pennsylvania State University National Center for Atmospheric Research (PSU NCAR) mesoscale model version 4 (MM4), which is described in detail by Anthes et al. (1987). The usual meteorological data plus the boundary layer fluxes were output every 3 hours. The version of the model used for this study utilized 14 vertical layers from the surface to 100 mb, periodic east-west boundaries, a β - plane variation of the Coriolis parameter, and the high resolution boundary layer model. The boundary layer occupies five of the 14 layers, with the lowest layer within the surface layer.

Differential friction can result from the boundary layer structure and processes in the model since the model vertical heat, moisture, and momentum fluxes use a vertical diffusion coefficient that depends on the local bulk Richardson number (R_b). The boundary conditions are considered stable when the bulk Richardson number (R_b) is greater than zero and Z_H/L is large. Z_H is the height of the surface layer and L is the Monin-Obukhov length. For very stable conditions ($R_b \geq 0.2$ and Z_H/L unrestricted), no turbulent fluxes occur. For stable conditions ($0.0 < R_b < 0.2$ and Z_H/L unrestricted), damped mechanical turbulent fluxes occur, and for marginally unstable or neutral conditions ($R_b < 0.0$ and $Z_H/L \leq 1.5$), both mechanical and buoyant turbulent fluxes occur. Unstable boundary conditions apply when both $R_b < 0.0$ and $Z_H/L > 1.5$, and under these conditions the vertical fluxes are computed using a convective plume model. Included in the fluxes is a downward entrainment flux at the top of the mixed layer equal to 20% of the surface flux.

Cloud formation and precipitation are parameterized through both non-convective and convective processes. Stable lifting that results in relative humidities greater than 100% is treated as non-convective precipitation, and the latent heat is added directly to the thermodynamic equation. Unstable ascent or convection is parameterized using a modified Kuo (1974) scheme (Anthes 1977) which redistributes the moisture and latent heat vertically through prescribed profiles. The criteria for convection are total column moisture convergence greater than 0.01 g m^{-2} s^{-1} and the predicted cloud height greater than 700 mb.

Diabatic heating used in the Sawyer-Eliassen diagnostic equation is computed as the residual of the thermodynamic equation

$$Q = \frac{d\theta}{dt} = C_p\left(\frac{\partial T}{\partial t} + V \cdot \nabla_H T + \omega \frac{\partial T}{\partial p}\right) + \alpha\omega$$

where

$$\theta = T\left(\frac{p_o}{p}\right) \exp \frac{R}{C_p}$$

The time tendency was computed as a six-hour time difference and introduces some error into the diabatic heating values. However, the diabatic heating data does correspond with the rainfall regions, giving at least qualitative confidence in their distribution. Because frictional forcing is computed as a second order vertical differential, forcing at the surface is represented by forcing at a level above the surface in the middle of the PBL.

B. INITIAL CONDITIONS

The initial sea-level pressure (SLP), surface equivalent potential temperature, and observed wind field for the three cases are shown in Fig. 8. The initial baroclinic instability conditions are the same in each case, with the only differences due to the respective surface heat and moisture flux distributions. The initial model cyclone differs from an actual atmospheric cyclone most significantly in its lack of an initial vertical circulation, its moisture structure being too dry compared with typical cloud patterns of actual cyclones, and a slight upshear tilt in the thermal wave. All but the moisture distribution difference are eliminated in the first six hours of each model simulation. The moisture distribution takes 18 hours to resemble the typical cloud pattern of an actual cyclone, which also gives less certainty to the diabatic heating contributions to the model cyclogenesis and frontogenesis.

The control experiment (Case 1) uses a zonal SST distribution (Fig. 9) and includes surface heat and moisture fluxes throughout the simulation. With this SST distribution the mean baroclinicity in the atmosphere is reinforced, and the pattern of surface heating introduces temperature tendencies that counteract the initial thermal advection (Nuss and Anthes, 1987). The initial surface flux distribution is characterized by upward heat and moisture fluxes west of the surface low and downward fluxes east of the surface low. The second experiment (Case 2) uses the same zonal SST distribution but insulates the atmosphere from the sea surface by specifying a zero heat and moisture flux condition

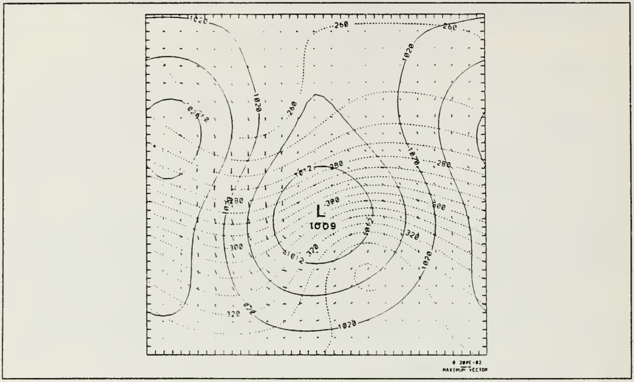

Fig. 8. **Initial conditions.** SLP in mb (solid), θ_e in K (dashed), and observed wind vectors in m s^{-1} for each case. Length of wind vector denotes intensity, with the maximum length representing 50 m s^{-1}.

throughout the simulation. Because the only source of moisture in the model is from the surface moisture flux, this case has no moisture directly transported to mid and upper levels as in the other two cases, and relies on the cloud formation and precipitation parameterization applied to rising warm air cooled through adiabatic processes. The downward momentum flux is not specifically modified from Case 1, except indirectly through stratification effects that result from no surface heating. With no surface fluxes, the total frictional convergence is reduced to that caused by differential downward momentum fluxes, and there is no thermal damping effect in the boundary layer.

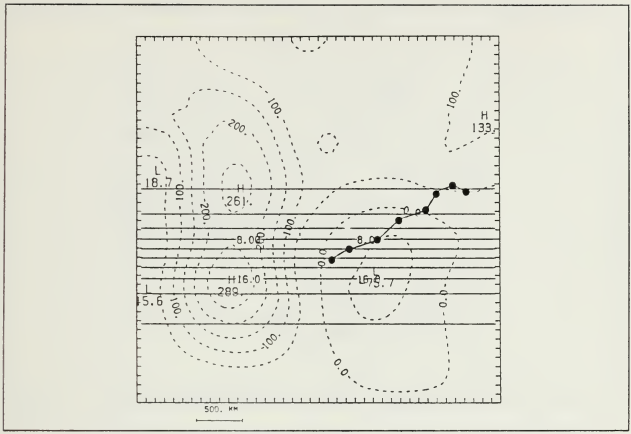

Fig. 9. Case 1 and Case 2 SST distribution. SST in °C (solid), with the initial total (latent plus sensible) heat flux distribution in W m^{-2}, and the cyclone track and position at six-hour intervals from 00 h to 48 h indicated for Case 1.

The final experiment, Case 3, uses a sinusoidal SST distribution and includes surface heat and moisture fluxes as in Case 1 (Fig. 10). The sinusoidal SST distribution in this case is in phase with the thermal structure of the cyclone, thus reinforcing the low-level baroclinicity instead of the large scale mean baroclinicity. This distribution results in large upward total heat fluxes to the northeast of the surface low as well as to the west. In this case the magnitude of the heat flux is largest northeast of the surface low, enhancing the frictional convergence northeast of the surface low compared with Case 1.

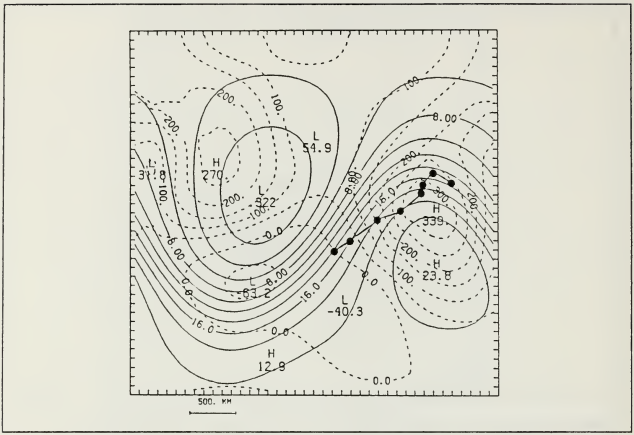

Fig. 10. As in Fig. 9, except for Case 3.

C. DEVELOPMENT OF THE CYCLONE

The differences in structure and dynamics of each cyclone throughout the simulations represent the direct and indirect effects of the surface flux distribution unique to each case, since the initial baroclinic instability factors are identical. The intensity of cyclogenesis in each case can be described in part by the sea-level pressure (SLP) deepening rate. Fig. 11 is a plot of the lowest closed contour of SLP around the center versus time for each case. By the Sanders and Gyakum (1980) definition of explosive development (1 mb h^{-1} for 24 h or more), all three cyclones develop explosively, with the average deepening rate 1.46 mb h^{-1} for Case 1, 1.89 mb h^{-1} for Case 2, and 1.65 mb h^{-1} for Case 3 (Nuss and Anthes 1987).

In Case 1, the cyclone tracks northeast towards colder water, initially over a region of increasing downward heat fluxes, and then towards the region of increasing upward heat fluxes in the top right quadrant of Fig. 9. As the cyclone moves towards this region, the differential in static stability across the warm front is enhanced. Increased

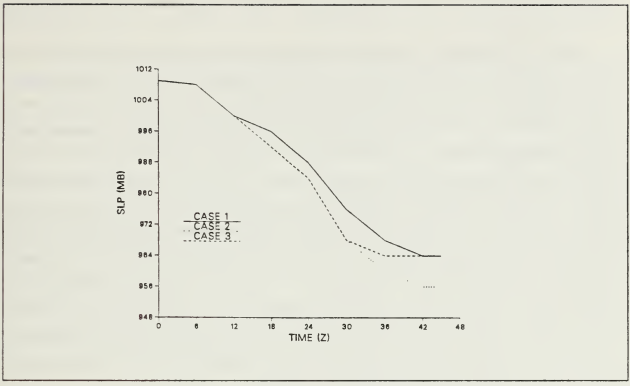

Fig. 11. **SLP (mb) versus time for each case.** Note that the deepening rates are the same for each case until 12 h, and the deepening rates of Cases 2 and 3 are equivalent until 30 h.

upward heat fluxes ahead of the front reduce the static stability in this region compared with the comparatively small increase in static stability behind the front in the region of downward heat fluxes. Differential static stability in the PBL increases frictional convergence, however it is small relative to the thermal damping effects of the heat flux distribution, which acts to slow frontogenensis by warming the cold air sector ahead of the front and cooling the warm air sector behind the front. This prevents the formation of concentrated temperature gradients at the surface and associated strong temperature advection (Nuss and Anthes, 1987).

The removal of surface heat and moisture fluxes in Case 2 results in an increased rate of cyclogenesis compared with Case 1. In the absence of surface fluxes, differential static stabilty across the front is reduced, so frictional convergence due to differential downward momentum fluxes is no longer enhanced. However, the frontolytical thermal effect of the Case 1 surface heat fluxes is removed, and indeed, Nuss and Anthes (1987) showed that the low-level thermal cold and warm front advection increased in this case

compared with Case 1, and the temperature gradients were stronger, indicating stronger cold and warm fronts.

In Case 3 the cyclone tracks northeast across the SST gradient, moving slightly towards warmer water until the 24 hour point (24 h) when the cyclone starts tracking towards colder water. This track results in an initial reduction in downward fluxes east of the surface low until 24 hours, when the downward fluxes begin to increase as the cyclone changes direction. The surface flux distribution of the first 24 hours favors a maintenance of the baroclinicity of the cyclone. The distribution of strong upward fluxes north of the warm front results in reduced low level static stability and stronger heating of the PBL in this region, which enhances frictional convergence northeast of the surface low. The frictional convergence in this case is stronger than in Case 1, where the upward heat fluxes northeast of the surface low were not as strong. Another significant difference between the two cases is that the moisture flux to the northeast of the warm front in Case 3 is greater than 200 W m^{-2} compared with near zero in the control case (Nuss, 1989), and there is an upward moisture flux throughout most of the warm sector in Case 3 compared with near zero fluxes in Case 1.

As discussed by Nuss (1989), convergence near the cyclone center and warm front play a significant role in the vertical circulation of the cyclone. Because of the heat flux distribution, stronger wind stress results to the northeast of the surface low in Case 3 compared with Cases 1 and 2. The curl of the surface stress is proportional to the frictional PBL convergence (Fleagle and Nuss, 1985). With increased convergence into the surface low and warm front in Case 3 as a result of the stronger heating, the PBL ageostrophic flow toward the front and low is strongest in this case. This results in a stronger low-level transverse component of the secondary circulation, which in turn enhances the intensity of the cold conveyor belt flowing towards the cyclone ahead of the warm front, which transports boundary layer air that has been heated and moistened by the surface heat fluxes toward the cyclone center. The result is increased vertical transport of heat and moisture out of the boundary layer, contributing to stronger midtropospheric heating and greater intensification of the cyclone than in Case 1. In both Cases 1 and 3, the strongest ascent was found to be along a line extending from the cyclone center southeast and along the warm front. In Case 3, both the frictional convergence and latent heat release are offset by the frontolytical effect of the surface heat flux distribution after 24 h. It appears that the reduction in the deepening rate of the cyclone can be related to the removal of the favorable conditions of the first 24 hours. It remains to be shown whether the stronger frictional convergence in Case 3 is due to

PBL processes or stronger geostrophic forcing that results from other indirect effects of the surface fluxes.

The role of surface heat and moisture fluxes in oceanic cyclogenesis is complex. The frontogenetical effects of surface heat fluxes on the PBL stratification and frictional convergence are opposed by the direct frontolytical effects on the thermal gradient. On the other hand, turbulent mixing can transport heat and moisture out of the boundary layer into the troposphere where it can enhance the temperature gradient through the release of latent heat. This feeds back to the cyclone, since the enhanced thermal gradient enhances the secondary circulation and intensity of the cyclone, which in turn enhances the winds and the geostrophic frictional convergence. It can be seen that the advance of the cyclone into a new distribution of differential heat and moisture fluxes has a critical impact on the intensity of cyclogenesis. Case 1 allows an analysis of boundary layer processes in the presence of a continuously changing cross-front SST distribution. Case 2 allows analysis of frontogenesis and cyclogenesis in the absence of surface heat and moisture fluxes, and Case 3 allows analysis of these processes in the presence of an initially uniform SST gradient followed by a changing gradient after 24 hours of development.

D. TOTAL FORCING AT THE SURFACE

The intensity of the surface warm front can be represented by the total geostrophic and ageostrophic forcing at the surface. Figs. 12 and 13 show the total forcing at the surface at 24 h for Cases 1 and 2, and Fig. 14 shows the same for Case 3. Recalling the direction of flow around vertically-oriented centers of positive and negative forcing as discussed in Section II, one can determine the sense of flow in the vertical plane from the sign of the forcing at the surface. In each case there is a region of slightly negative forcing ahead of the warm front, which implies clockwise circulation in the vertical plane and consequently flow towards the northeast in the horizontal plane of the surface. Similarly, the regions of positive forcing imply counterclockwise circulation in the vertical plane, and consequently surface flow towards the southwest. The vertical plane of flow is assumed to be perpendicular to the axis of horizontal forcing, and the sign of the forcing at the surface is assumed to extend vertically above that region.

The boundaries between the positive and negative regions of forcing are of particular importance since they represent the transition from counterclockwise to clockwise flow, and hence are regions of upward or downward vertical motion. For example, in Case 3, the boundary between the negative region to the northeast of the front and the posi-

tive region within the surface front is a downward vertical motion region. Similarly, the boundary between this positive region and the negative region south of the surface low is an upward vertical motion region. This combination of downward motion ahead of the front and upward motion behind the front supports the direct circulation and is frontogenetical in that the forcing enhances the temperature gradient. The strongest surface flow is to the southwest, perpendicular to the axis of forcing, which is close to the position of the warm front.

The total forcing is strongest in Case 2 and weakest in Case 1, which supports the results of Nuss (1989), who found that the Case 2 warm front was the strongest. Yet this case did not have the strongest vertical circulation or cold conveyor belt, nor did it have the most rainfall, although it had the most intense cyclone. The structure of the vertical circulation and forcing above the surface is not necessarily the same as that of the surface. A clearer picture can be obtained from an analysis of the cross-sections of total forcing for each case. Of more importance is how each component of forcing is contributing to the total forcing at all levels, and what effect the surface fluxes have on these components.

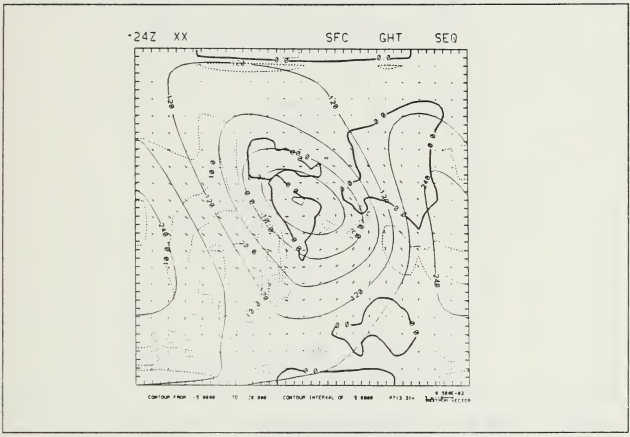

Fig. 12. Total forcing at the surface at 24 h, Case 1. Geopotential height in m (solid), total forcing in K 100 km^{-1} day^{-1} (dashed), and observed wind vectors in m s^{-1}. Wind vectors vary in length according to speed, with the maximum length 50 m s^{-1}. Contour interval of forcing is 5. Heavy lines denote zero contours.

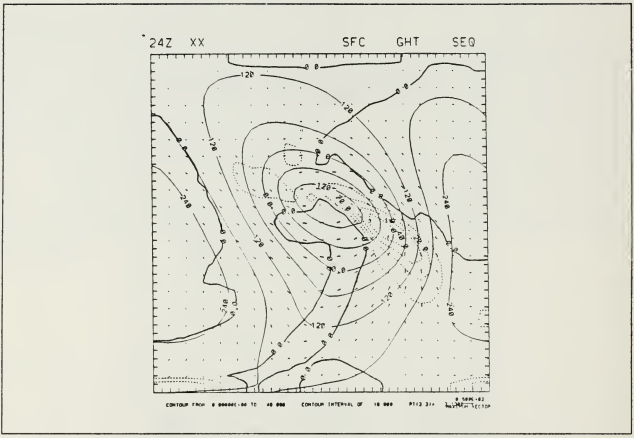

Fig. 13. As in Fig. 12, except for Case 2. Contour interval is 10.

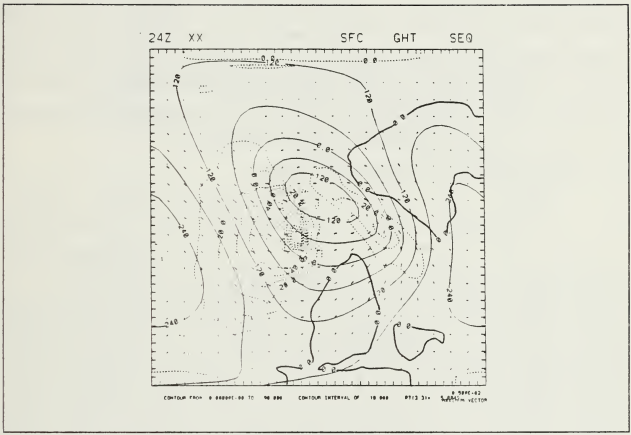

Fig. 14. As in Fig. 12, except for Case 3. Contour interval is 10.

IV. RESULTS

A. OVERVIEW

A series of surface plots of total frontogenetical forcing through the cyclone domain were taken at six-hour intervals to analyze the evolution of total forcing. Figs. 12 through 14 are representative of the general pattern and relative intensities of forcing of the cold and warm fronts observed throughout the simulations. Although there is positive forcing of the warm front in each case, total forcing at the surface in Cases 1 and 3 is strongest in the cold air sector behind the cold front, whereas in Case 2 total forcing is strongest in the vicinity of the warm front. This suggests that processes unique to Cases 1 and 3 are dominating total forcing at the surface.

B. TOTAL FORCING OF THE WARM FRONT

1. Surface

As seen in Figs. 12 through 14, the pattern of forcing of the warm front in Cases 2 and 3 is elliptical, whereas a distinguishable ellipse of forcing does not become evident until 30 h in Case 1. Total forcing reaches a maximum at 30 h in Case 3, and 36 h in Cases 1 and 2. Fig. 15 is a time series of the total forcing of the warm front, measured as the maximum contour value at the approximate mid point of the surface warm front. This is in the location of maximum forcing, and also avoids the occluded front. Total forcing reaches a maximum of 10 K 100 km^{-1} day^{-1} in Case 1, 40 K 100 km^{-1} day^{-1} in Case 3, and 100 K 100 km^{-1} day^{-1} in Case 2. Comparing the SLP deepening rates from Fig. 11 with the rates of growth and relative intensities of total forcing from Fig. 15 for each case, one can see that the strongest frontogenetical forcing and deepest cyclone are both in Case 2, and the weakest total forcing and slowest deepening rate are in Case 1.

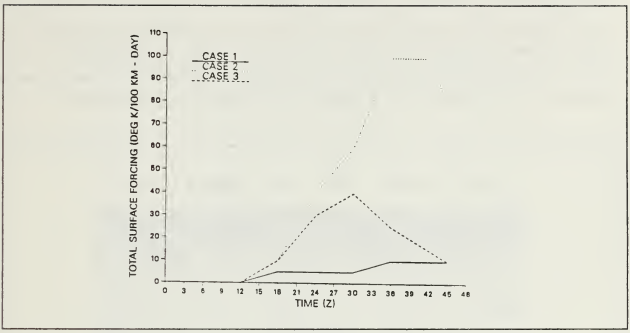

Fig. 15. Evolution of total forcing of the surface warm front.

2. Cross Sections

Cross sections of total forcing of the warm front were taken at six-hour intervals for each case, oriented perpendicular to the warm front and bisecting the region of maximum total forcing of the warm front at the surface for that time. The cross sections depict more clearly the location of total forcing in the vertical plane with respect to the vertical circulation field and surface warm front. By 12 hours all three cases have broad regions of positive total forcing in the cold air sector ahead of the warm front, and generally negative forcing in the warm air sector behind the warm front. The counterclockwise circulation induced by the positive forcing ahead of the front, and the clockwise circulation induced by the negative forcing behind the front, set up the direct circulation cell and upward vertical motion region in the warm front, as suggested in Section II and as indicated in Figs. 16 through 18 by the vectors of ageostrophic vertical motion. Figs. 16 and 17 show the cross sections of total forcing at 24 hours for Cases 1 and 2, and Fig. 18 shows the same for Case 3. The orientation from left to right in the cross-sections is northeast to southwest, with the cold air sector ahead of the front to the left and the warm air sector behind the front to the right.

The initial model cyclone does not have an initial vertical circulation field; rather it evolves over the course of the simulation as frontogenetical processes occur in the model. The presence of a distinct updraft region, as depicted by the vectors of

ageostrophic flow around the warm front, is evident by the 12 hour point in Case 3, with a less distinct updraft region in Case 1 at this time. Case 2 does not develop a distinguishable updraft region until 18 hours. One can get a sense of the intensity of the cold conveyor belt (CCB) from the magnitude of the ageostrophic vectors circulating around the direct cell in each case. The strongest CCB is in Case 3, while the weakest is in Case 2.

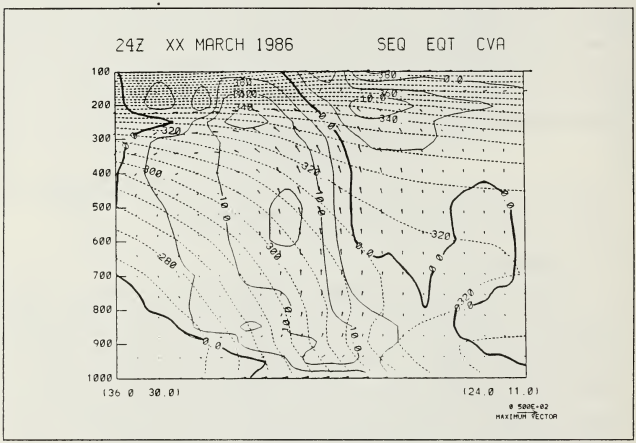

Fig. 16. **24-h cross section of total ageostrophic forcing, Case 1.** Forcing is in K 100 km^{-1} day^{-1} (solid), θ_e in K (dashed), and ageostrophic circulation vectors. Ageostrophic circulation vectors vary in length according to speed, with the maximum length corresponding to 50 m s^{-1} in the horizontal and 50 μb s^{-1} in the vertical. Heavy lines denote zero contours. Contour interval of forcing is 5.

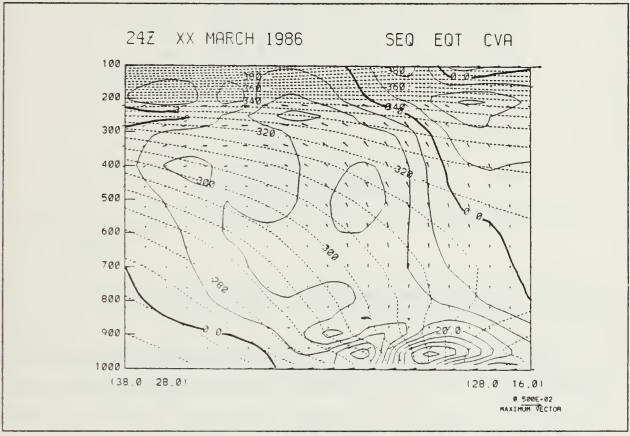

Fig. 17. As in Fig. 16, except for Case 2. Contour interval is 5.

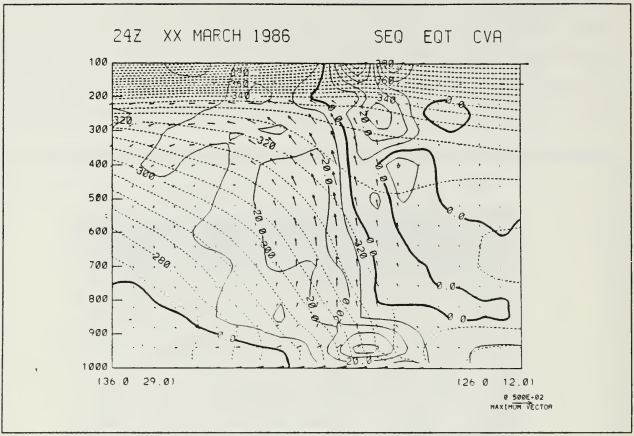

Fig. 18. As in Fig. 16, except for Case 3. Contour interval is 10.

By the 18 hour point Cases 1 and 3 have distinguishable ellipses of positive total forcing extending vertically within and ahead of the updraft region, whereas in Case 2 a similar region is not apparent until 24 hours. Cores of positive forcing in the boundary layer are first distinguishable in Case 1 at 30 h, and at 24 h in Cases 2 and 3, after which the boundary layer remains the level at which total forcing is the strongest. Of all the cases, Case 2 develops the strongest boundary layer total forcing, reaching a maximum of 150 K 100 km^{-1} day^{-1} at 36 h. The relative maxima and times of occurrence in Cases 1 and 3 are 35 K 100 km^{-1} day^{-1} at 36 h and 60 K 100 km^{-1} day^{-1} at 30 h respectively. Fig. 19 shows the evolution of total forcing in the PBL for each case, measured from the respective cross sections as the maximum positive value in the core of positive forcing near the updraft region, typically at about 950 mb. Although this is a crude measure of the frontogenesis, it gives at least qualitative evidence of how the forcing evolves in each case. Case 3 has the strongest initial forcing, but is the case in which the PBL forcing first declines. Between 18 h and 24 h the total forcing in Cases 2 and 3 is the

same, after which the rate of growth begins to decline in Case 3 while the growth rate in Case 2 continues to increase.

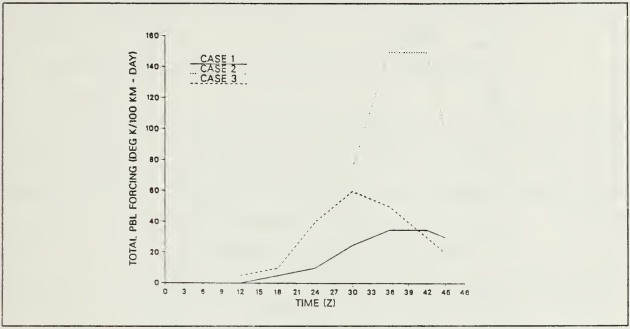

Fig. 19. Evolution of total forcing in the PBL.

At mid levels, Case 1 develops the strongest total forcing, reaching 35 K 100 km^{-1} day^{-1} at 42 h. Case 2 develops a maximum of 30 K 100 km^{-1} day^{-1}, and Case 3 develops a maximum of 20 K 100 km^{-1} day^{-1} at 24 h. Fig. 20 is a summary of the total forcing at mid levels, measured in the direct circulation cell as the maximum contour of positive forcing at 600 mb.

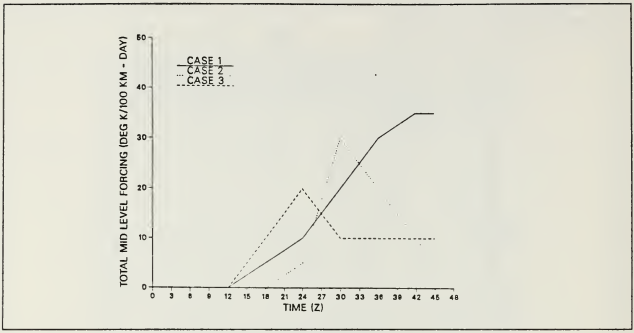

Fig. 20. Evolution of total forcing at mid levels.

C. TOTAL FORCING AT 24 HOURS

For continuity with Nuss (1989), the 24-hour time was chosen for detailed analysis. This time is representative of the most rapid phase of development, and is just prior to formation of the occluded front. By this time in the evolution, the effect of the fluxes will have influenced all the terms to some degree. In all three cases there is a large region of positive forcing ahead of the warm front, and generally negative forcing behind the front. The gradient of total forcing at mid levels is strongest in the updraft region where the vertical vectors are the strongest. The positive forcing in the direct circulation cell dominates the negative forcing, suggesting that the direct cell is the dominant cell in the secondary circulation of the warm front.

The patterns of forcing of the direct circulation cell in each case, as seen in Figs. 16 through 18, are not symmetrical ellipses as discussed in Section II, particularly in Cases 2 and 3 where there is a cell of strong positive forcing in the boundary layer beneath the updraft region. Case 1 develops a similar region by 30 hours. There are distinct differences in the forcing at each level in the three cases, and as discussed in the previous section, must be a result of the differences in the surface fluxes in each case. As described by Nuss (1989), different surface heat and moisture flux distributions resulted in differing rates of cyclogenesis, frontogenesis, and intensity of the cold conveyor belt. There is certainly evidence of a relationship between total forcing of the warm

front, especially at the surface, and the cyclone deepening rate. The important question is how these flux distributions, which differed primarily near the warm front, modified the warm frontal temperature gradient and vertical motion in each case, as indicated by differences in total forcing.

D. CONTRIBUTIONS BY EACH COMPONENT OF FORCING

1. Overview

The total forcing in each case is strongest in the boundary layer, with confluence and shear the dominant contributors to total forcing at this level. Confluent forcing is generally concentrated beneath the updraft region, with shear extending from this location into the direct circulation cell at low levels. Diabatic heating is generally negative at this level in all three cases, concentrated beneath the updraft region but extending ahead of the warm front as with shear. Frictional forcing is a small component of total forcing of the warm front. The forcing due to diabatic heating is the dominant component of total forcing at mid and upper levels, and generally located within and ahead of the updraft region. Centers of mid-level confluence and shear are located within the direct cell ahead of the warm front. Interesting departures from these general results were found in each case, as described below.

2. Case 1

The 24-h sensible and latent heat flux distributions for Case 1 are shown in Fig. 21, with the positions of the front and cross-section added for reference. By this time the initial 1009 mb low has deepened to a 986 mb low, with strong positive total (latent plus sensible) heat fluxes west of the low and downward fluxes east of the low. This distribution prevents the formation of concentrated surface temperature gradients and strong temperature advection, since the upward fluxes are warming the cold air region and the downward fluxes are cooling the warm air region. However this effect extends only to the top of the boundary layer (Nuss and Anthes, 1987).

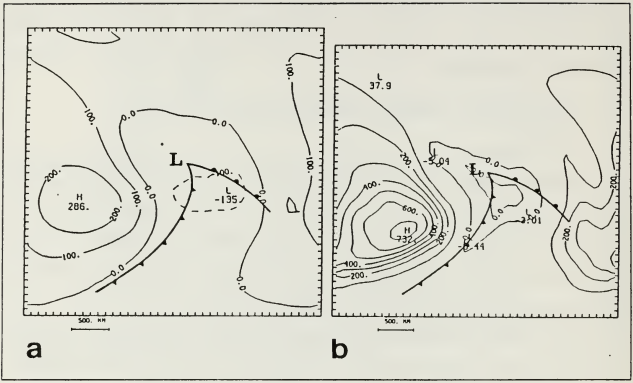

Fig. 21. **24-h heat flux distributions for Case 1.** (a) sensible and (b) latent heat flux distributions in W m^{-2}. Dashed lines indicate downward or negative fluxes. Fronts added for reference. From Nuss, 1989.

a. Surface

The frictional convergence and diabatic heating components of forcing for the surface are shown in Figs. 22 and 23. Frictional forcing is negative in the region of upward heat fluxes northeast of the surface low, but also slightly negative in the region of downward heat fluxes behind the warm front. However, the frictional forcing is strongly positive in the cold air sector behind the cold front where the upward heat flux is the strongest. The inconsistency of the frictional forcing relative to the sign of the heat fluxes suggests that the momentum fluxes in the model depend on other factors that are not determined simply from the fluxes. This may be particularly important when the boundary layer is close to neutral stratification.

The sense of the ageostrophic flow induced in the region of negative forcing northeast of the warm front is for surface flow to the northeast, with corresponding downward motion at the boundary between this region and the region of positive forcing closer to the front. Similarly, the induced flow in this region of positive forcing is to the

southwest, with downward flow along the boundary with the negative region to the northeast closer to the warm front. The boundary between this positive forcing region and the region of negative frictional forcing associated with the low and warm front is upward. The combined flow would tend to support the direct circulation cell as discussed in the previous section. The overall pattern of frictional forcing resembles the pattern of total heat fluxes. Over the course of the simulation the band of positive frictional forcing expands in size, although the magnitude does not substantially change. This suggests that as the cyclone becomes more intense and the geostrophic winds increase, downward momentum fluxes begin to influence frictional forcing more than they did initially, resulting in reduced negative frictional forcing.

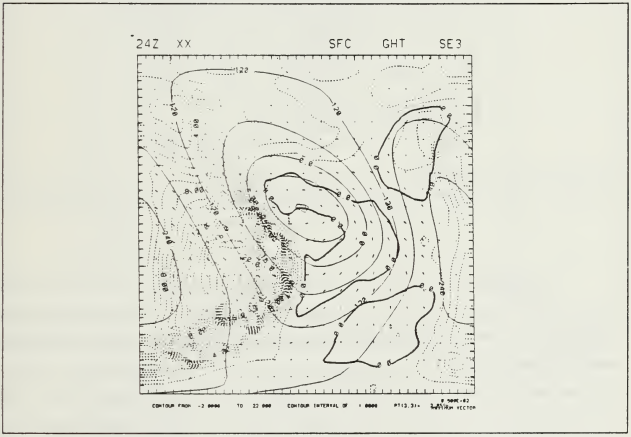

Fig. 22. 24-h surface forcing due to friction, Case 1. Forcing in K 100 km^{-1} day^{-1} (dashed), with geopotential height (solid) in m and observed wind vectors in m s^{-1}. Contour interval of forcing is 1.

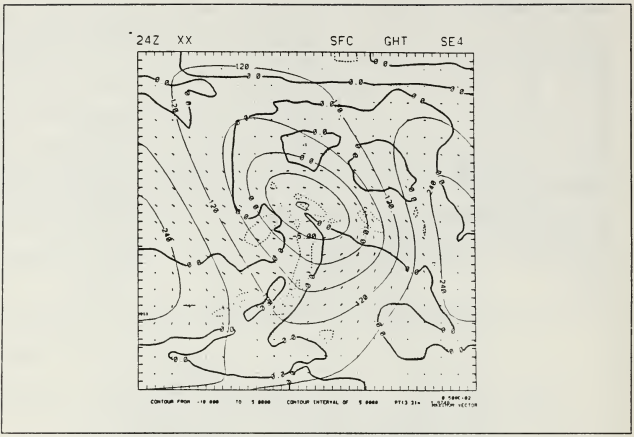

Fig. 23. 24-h surface forcing due to diabatic heating, Case 1. Contour interval is 5.

Forcing due to diabatic heating at the surface is frontolytical to the warm front, with the values of forcing larger than frictional forcing. Unlike the pattern of frictional forcing, the pattern of this component of forcing does not resemble the surface heat flux pattern, because the horizontal gradient of the heating is being considered. What is evident from Fig. 23 is that the surface heating gradient tends to reduce the low-level temperature gradient. The boundary between the negative forcing region along the warm front and the positive forcing region behind the front implies downward motion along the warm front. Consequently, there is opposition of the surface warm frontogenesis and secondary circulation. The diabatic heating component dominates any frontogenetical effect of the frictional forcing, giving a net frontolytical effect of the boundary layer processes at this time.

b. Cross-Sections

The cross-sections in Figs. 24 and 25 depict the vertical extent of these diabatic forcing terms. Frictional forcing extends up to 900 mb in the model, at which point boundary layer stresses are zero. In Fig. 24, the sense of flow between the positive region of frictional forcing ahead of the updraft region and the negative region beneath the updraft is frontogenetical, supporting the leading edge of the updraft region.

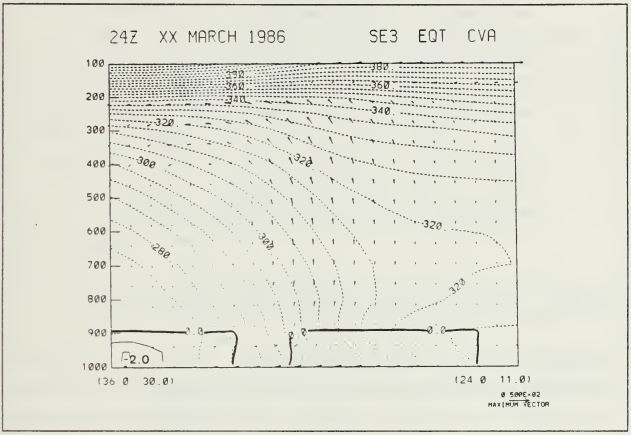

Fig. 24. 24-h cross-section of frictional forcing, Case 1. θ, in K (dashed), ageostrophic vertical circulation vectors in $\mu b\ s^{-1}$, and ageostrophic forcing in K 100 $km^{-1}\ day^{-1}$ (solid). Contour interval is 1. Heavy lines denote zero contours.

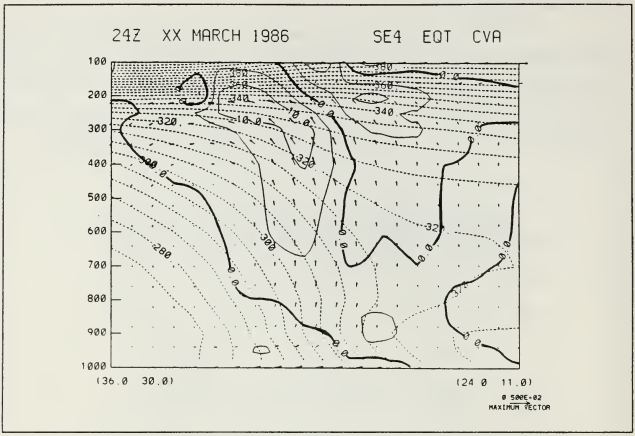

Fig. 25. As in Fig. 24, except for diabatic heating. Contour interval is 5.

The boundary between the negative and positive regions of diabatic forcing beneath the updraft region in Fig. 25 is frontolytical, and dominates frictional forcing as mentioned above. However, this frontolytical component of forcing is dominated by positive values of shear and confluent geostrophic deformational forcing (not shown) in the boundary layer ahead of the front. At mid and upper levels diabatic heating generates frontogenesis and supports forcing of the updraft region throughout its vertical extent. The transport of heat and moisture from the surface to the mid and upper levels allows for latent heat to be released within and behind the warm front, which enhances the temperature gradient in the warm air sector. Because the forcing is positive it also enhances the secondary circulation. Geostrophic deformation is also positive at mid levels, although diabatic heating dominates, especially near the updraft region. The diabatic forcing is most susceptible to error at upper levels where the horizontal temperature gradient is a minimum, so a further discussion of upper-level forcing is precluded, and is not the focus of this study.

3. Case 2

By 24 h the cyclone in this case has deepened to 984 mb. Although it has the strongest warm front, it has about the same accumulated rainfall as Case 1 for this time, and also has the weakest secondary circulation and CCB. The patterns of confluent and shear geostrophic deformation are similar to Case 1 and are presented for this case for reference.

a. Surface

Figs. 26 and 27 depict the surface forcing due to confluent and shear geostrophic deformation, and is representative of the typical pattern of this forcing seen in Case 1 after 24 h. Fig. 28 depicts the forcing due to diabatic heating at the surface. With the absence of surface heat and moisture fluxes in this case, frictional forcing is negligible, suggesting that surface heat fluxes play a significant role in driving the downward momentum flux. Although there are no surface heat and moisture fluxes in this case, the pattern of forcing due to diabatic heating at the surface is similar to that of Case 1, with stronger values. This suggests that either the errors in the diabatic heating calculation are relatively large or that there are significant differences in the boundary layer parameterization in the model.

The sense of how the positive and negative regions of forcing enhance or retard the secondary circulation is the same as in Case 1. Again, the boundary between the band of positive forcing near the warm front in Fig. 28 and the broad negative region to the northeast of the front is a downward motion region. Similarly the boundary between this positive region and the negative region near the surface low is upward. As in Case 1, this is frontolytical.

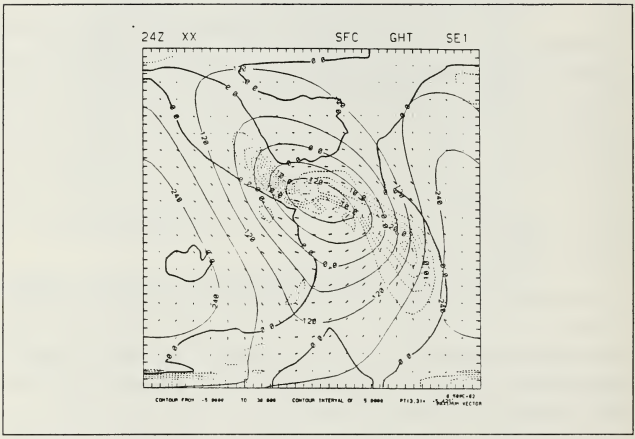

Fig. 26. 24-h confluent geostrophic forcing at the surface, Case 2. Contour interval is 5.

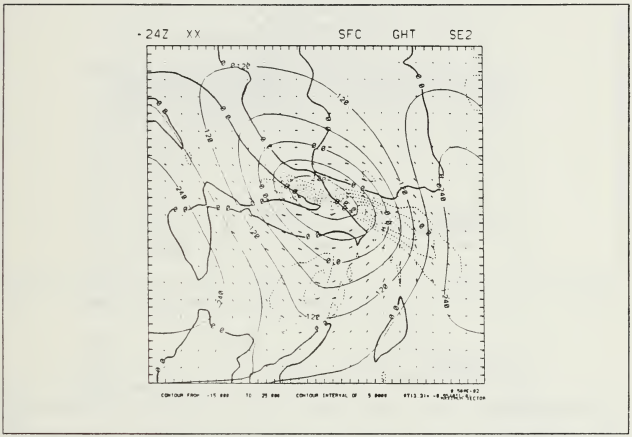

Fig. 27. As in Fig. 26, except for forcing due to shear. Contour interval is 5.

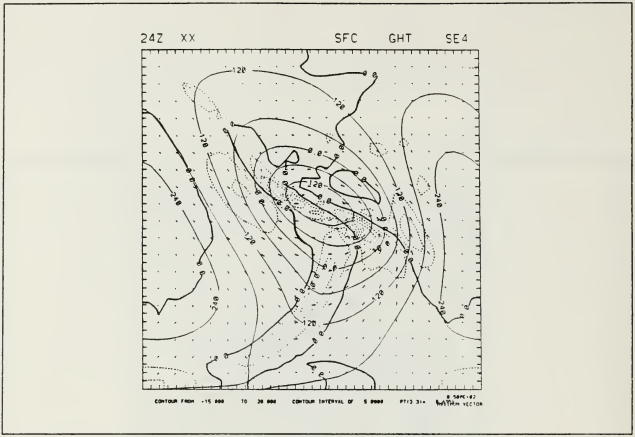

Fig. 28. As in Fig. 26, except for diabatic heating. Contour interval is 5.

b. Cross-Sections

The strength of the vertical circulation is weaker in this case than in Case 1, as indicated by the vertical velocity vectors of Figs. 29 through 31. Confluence and shear, in Figs. 29 and 30 respectively, are strongest in the boundary layer beneath the updraft region. In Fig. 31, diabatic heating at mid levels, in the form of latent heat, is not as strong as in Case 1. This is to be expected since the only direct source of moisture in the model is from the PBL. Not only is there no frictional confluence, there is no moisture transported by the CCB to surface low. In addition, the weaker secondary circulation in this case supports the weaker CCB found by Nuss (1989). However, this case is dominated more strongly by geostrophic deformation at the surface than Case 1, which supports the findings in previous studies that geostrophic deformation dominates frontogenesis and cyclogenesis, since this case has the strongest warm front and eventually the deepest cyclone.

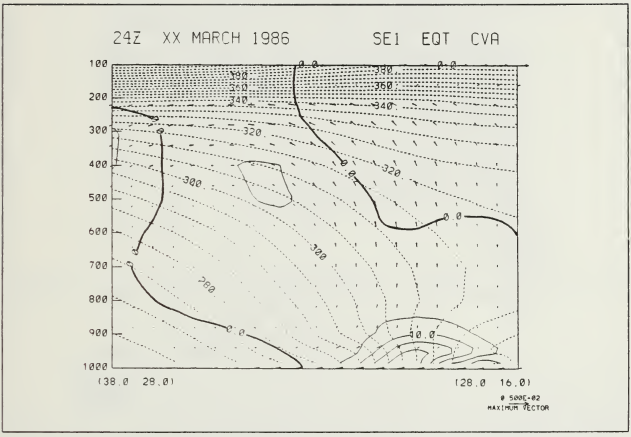

Fig. 29. **24-h cross-section of confluent geostrophic forcing, Case 2.** Contour interval is 5.

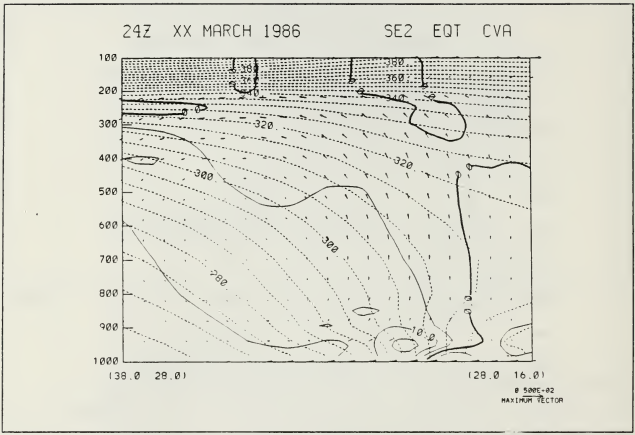

Fig. 30. As in Fig. 29, except for forcing due to shear. Contour interval is 5.

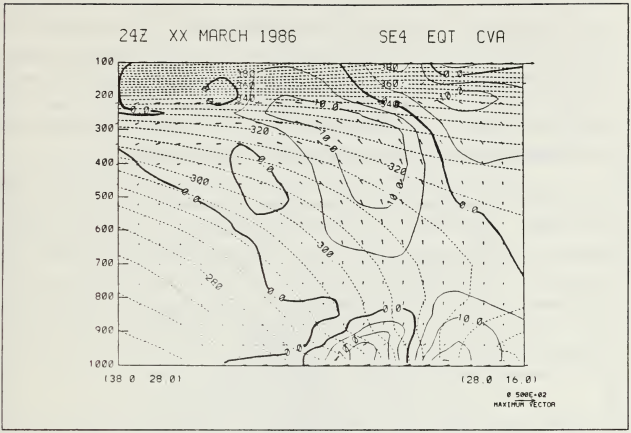

Fig. 31. As in Fig. 29, except for diabatic heating. Contour interval is 5.

4. Case 3

The cyclone in this case has developed as rapidly as the Case 2 cyclone, and although the surface front is not as intense as in Case 2 it has the most accumulated rainfall at 24 h. The heat flux distribution at 24 h, as shown in Fig. 32, is characterized by strong upward heat fluxes behind the cold front, positive heat fluxes northeast of the surface low and warm front, and a pocket of downward heat fluxes near the trailing edge of the center of the warm front, similar to Case 1.

a. Surface

The pattern of frictional forcing in Case 3, as shown in Fig. 33, is quite different to that of Case 1, in that almost the entire region east of the surface low is negative. Within this negative region is a pocket of slightly positive frictional forcing near the warm front. Again, the frictional forcing distribution is more complex than the heat flux pattern, indicating the significance of other factors. Whereas in Case 1 the region of positive forcing was ahead of the warm front, in this case it is located behind

the warm front. The resultant forcing of the flow between the positive and negative regions does not seem to located in the same position relative to the warm front to enhance the direct circulation cell and frontogenesis. As in Case 1, this region of positive frictional forcing expands in size, although not in magnitude. The magnitude of negative frictional forcing does increase slightly, although it decreases in area. This latter result was not seen in Case 1, and suggests that since the two cyclones are of equal intensity at this time, the difference is due to the surface heat flux distribution.

The 24-h surface diabatic heating in this case, as seen in Fig. 34, is similar to the other cases, but with a more narrow band of negative forcing associated with the warm front. The strength of the gradient from the negative to positive regions is strongest in this case, supporting a stronger transverse flow and vertical flow at the boundaries. Just as frictional forcing appears to be less frontogenetical than in Case 1, the locations of the upward and downward motion regions appear to be less frontolytical than in the other two cases. An analysis of the cross sections yields a clearer picture of this relationship.

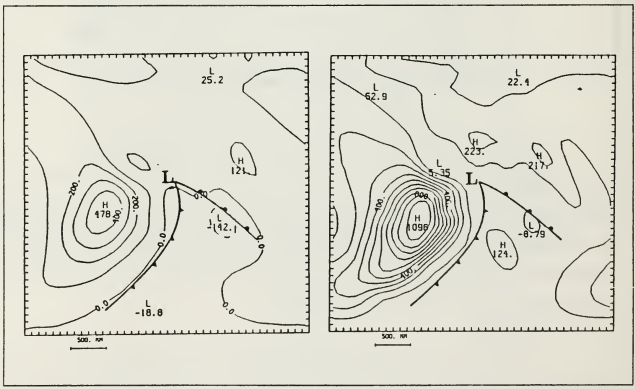

Fig. 32. As in Fig. 21, except for Case 3.

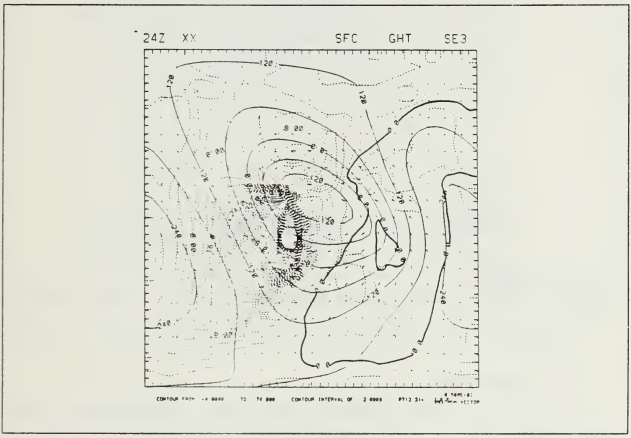

Fig. 33. 24-h surface forcing due to friction, Case 3. Contour interval is 2.

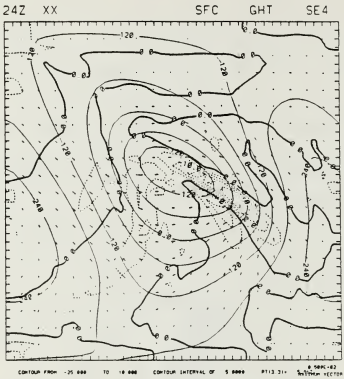

Fig. 34. 24-h surface forcing due to diabatic heating, Case 3. Contour interval is 5.

b. Cross-Sections

The cross-section of frictional forcing in Fig. 35 reveals that the region of positive frictional forcing is located beneath the trailing edge (warm sector side) of the direct circulation cell updraft region, with negative forcing directly beneath and ahead of the updraft region. The resultant vertical motion between these centers of forcing acts to oppose the vertical component of the direct circulation cell. However, because the negative frictional forcing ahead of the front is strongest in this case compared with Case 1, one can imagine a stronger transverse flow towards the front and cyclone at the top of the PBL. Thus frictional forcing is not enhancing the updraft region but is enhancing the transverse component of the direct circulation cell at low levels.

This case has stronger values of mid level latent heat than the other two cases at this time, as seen in Fig. 36, and indeed, this case has the most rainfall accumulation at 24 h. This suggests that the region of strong upward moisture flux northeast

of the surface front has influenced the latent heat of the mid troposphere, transported to the front and cyclone by the influence of frictional forcing.

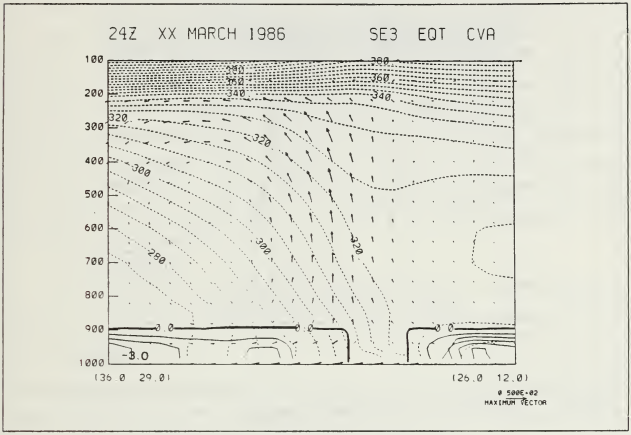

Fig. 35. 24-h cross-section of frictional forcing, Case 3. Contour interval is 1.

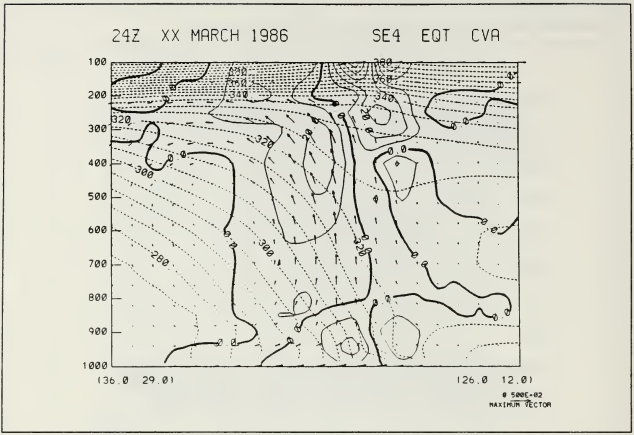

Fig. 36. As in Fig. 35, except for diabatic heating. Contour interval is 10.

E. TIME SERIES OF FORCING

The results at 24 h are a snapshot at one time, and the feedback of the surface diabatic effects on geostrophic forcing has not been separated. A time series of the contribution to total forcing by each component at low, mid, and upper levels attempts to separate the influence of each forcing term as they evolve throughout the simulation. Forcing was measured as the maximum value of each term along a horizontal line across the direct circulation cell in the respective cross-sections of each case. The most ambiguous term at low levels is the frictional forcing term. Frictional forcing was measured as the maximum positive value near the leading edge of the updraft region of the direct circulation cell, since this would enhance the updraft region in this location. This depiction does not take into account the influence of the negative frictional forcing ahead of the warm front. Theoretically, the clockwise circulation around the negative forcing center is acting to enhance the low-level transverse component of the circulation cell at the top of the PBL where the circulation around the region is towards the front and

cyclone. Forcing due to diabatic heating was measured as the maximum negative value at the base of the updraft region, since it was generally frontolytical in each case at this level and location. Confluence and shear were measured as the maximum positive values in the direct circulation cell within and ahead of the front. The 950 mb level was chosen since it is the level of maximum values for most of the terms at each time. At mid levels, the 600 mb level was chosen to represent the forcing due to confluence, shear, and latent heat release. Mid-level forcing was found to be a maximum at this level, with confluence and shear generally centered within the direct circulation cell, and latent heating located within the updraft region. Because the upper-level diabatic forcing is most susceptible to error, the maxima were located at 300 mb, where the center of the upper-level transverse component is located in each case. For reference, the SLP deepening rate is also provided with the 950 mb time series in each case.

1. **Boundary Layer**

The time series of forcing in the boundary layer for Cases 1 and 2 is depicted in Fig. 37, and for Case 3 in Fig. 38. In all three cases, confluent and shear geostrophic deformational forcing dominate total forcing at low levels, with confluence dominating shear throughout the simulations except for Case 1, where shear dominates confluence. Total forcing does not peak until 30 h in Case 3 and 36 h in Cases 1 and 2. This is consistent with the decline in the deepening rate of the cyclone in each case at these times. Surface diabatic heating is frontolytical, initially peaking at the same time as geostrophic forcing. This component of low level forcing is frontolytical in all three cases, and reduces total forcing by about 20 %. Unlike geostrophic deformational forcing, diabatic heating at the surface does not have a single peak and period of decline. Frictional forcing is not a significant contributor to total forcing in Cases 1 and 3, but it is the first component of total forcing to develop in Case 3. In all three cases, confluent and shear geostrophic deformational forcing and diabatic heating do not develop at low levels until after 12 h in Case 3 and 18 h in Cases 1 and 2. The earlier development of geostrophic deformation in Case 3 is presumably due to the influence of the frictional forcing that was present from the beginning. The period of maximum development of geostrophic and diabatic forcing is between 18 h and 24 h in all three cases, and the period of decline is between 30 h and 36 h.

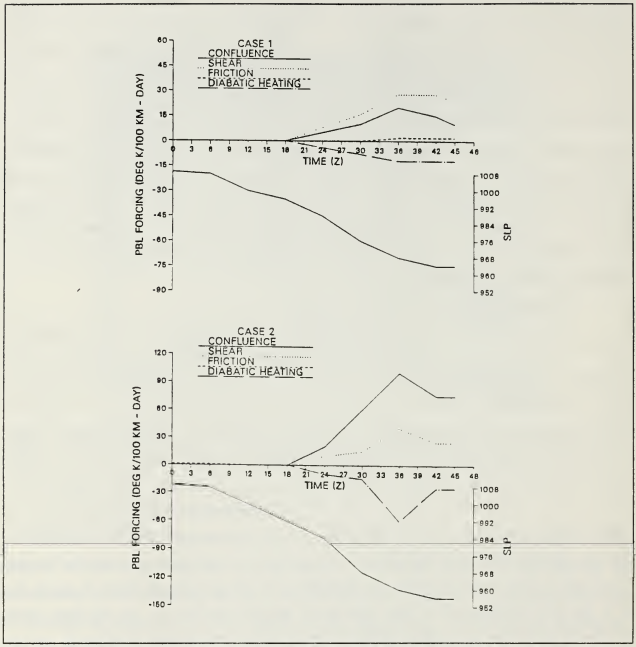

Fig. 37. Time series of forcing in the PBL. (a) Case 1, and (b) Case 2. Note the scale of forcing in Case 2 is twice that of Case 1.

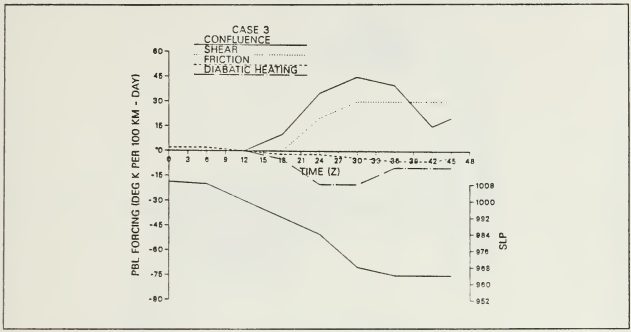

Fig. 38. As in Fig. 37, except for Case 3.

2. Mid and Upper Levels

The time series of total forcing at mid levels is depicted in Figs. 39 and 40. The time series for upper levels in depicted in Figs. 41 and 42. At both levels, diabatic heating dominates total forcing, except for Case 3 where geostrophic deformational forcing dominates. Mid level diabatic heating in the form of latent heat release is strongest in Case 1, where it does not peak and level off until 42 h, twelve hours after the deepening rate has begun to decline. In Cases 2 and 3 diabatic heating reaches a steady state at about 24 hours. At upper levels, there is some contribution to total forcing by confluent and shear geostrophic deformation. In Cases 1 and 2, diabatic heating at this level peaks at 36 h, then declines, whereas in Case 3 it remains steady after 24 h.

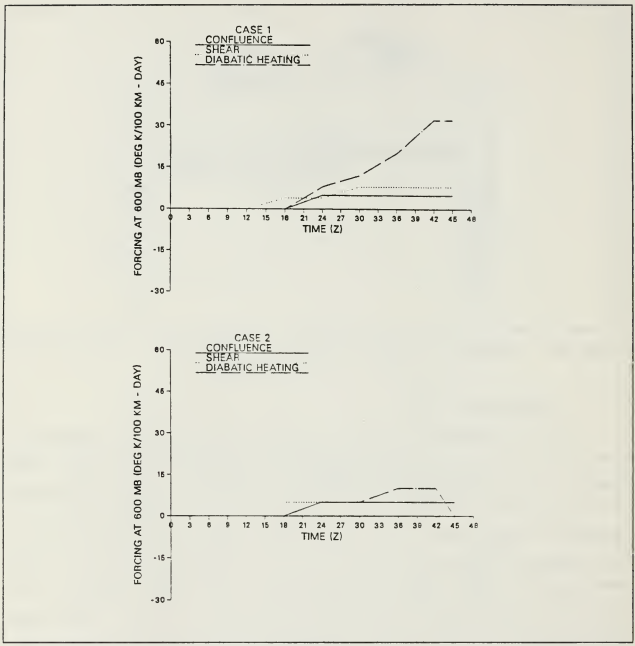

Fig. 39. As in Fig. 37, except for 600 mb.

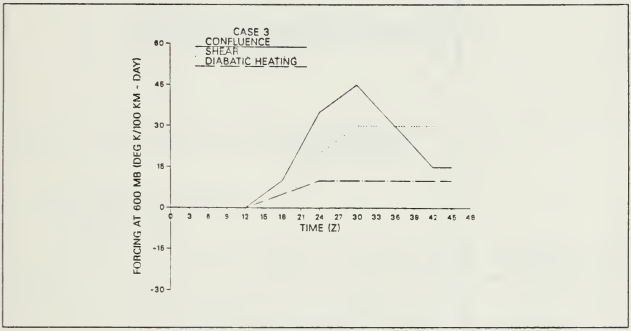

Fig. 40. As in Fig. 38, except for 600 mb.

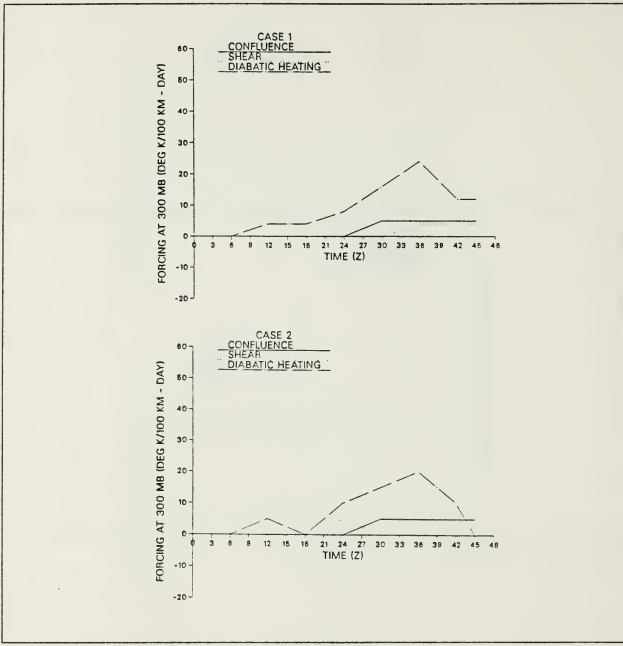

Fig. 41. As in Fig. 37, except for 300 mb.

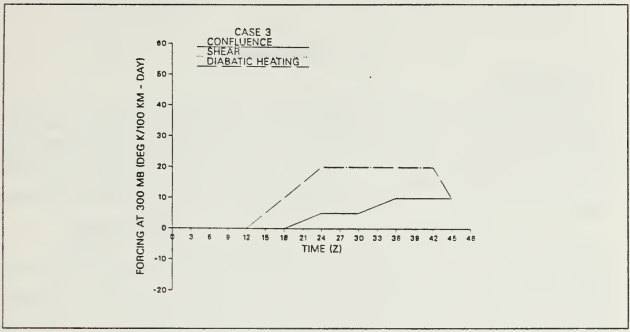

Fig. 42. As in Fig. 38, except for 300 mb.

F. COMPARISON OF CASES

1. Boundary Layer

Case 2 is similar to Case 1 during the first 18 hours, after which time the most significant differences are the rapid rise in geostrophic forcing in Case 2, the dominance of shear over confluence in Case 1, and the larger surface frontolytical effects of diabatic heating in Case 2. Comparing Case 3 with Case 1, the most significant differences are the stronger frictional forcing in the first 12 hours of development, the rapid rise in geostrophic forcing similar to Case 2 for the first 24 hours, and a decline in the frontolytical effects of diabatic heating after 30 hours.

2. Mid and Upper Levels

The most significant differences between Cases 1 and 2 are the steady rise in diabatic heating in Case 1 coupled with the presence of geostrophic forcing. There is no significant geostrophic forcing at mid levels in Case 2. In Case 3, latent heating is evident, but it not the dominant mid level forcing as it is in Case 1. Both confluent and shear deformational forcing dominate diabatic heating in Case 3. At upper levels, the only significant difference is the absence of any significant geostrophic deformational forcing in Case 2.

V. DISCUSSION

A. OVERVIEW

The basic conceptual model of frontogenesis is that geostrophic deformation forces strong frontogenesis at surface and upper levels, and at mid levels frontogenesis is usually weak and forced primarily by latent heat release. Frontogenetical forcing can be modified by small-scale frictional forcing and diabatic heating, with their relative contributions to frontogenesis modified by surface and boundary layer processes.

A review of the SLP deepening rates from Fig. 11 shows that for the first 12 hours each case deepens at the same rate, indicating that the surface flux distribution peculiar to each case does not have an apparent effect on frontogenesis until 12 h. None of the cases has significant geostrophic deformation enhancing the forcing during the first 12 hours, suggesting that small-scale processes of frictional forcing and diabatic heating in the boundary layer are important in setting the stage for the rate of development and structure of the cyclone and warm front. Once cyclogenesis has begun, forcing due to geostrophic deformation builds, which then feeds back on itself and dominates the forcing. In later stages, friction and diabatic heating act to modify the geostrophic deformational forcing.

B. BOUNDARY LAYER

1. Geostrophic Deformational Forcing

In their two-dimensional model simulation of frontogenesis, Baldwin et al. (1984) found that geostrophic deformation accounted for the large-scale features of the secondary circulation around a cold front, but was not the dominant forcing at low levels. Bond and Fleagle (1985) found similar results in their case study of an actual oceanic cold front. Baldwin et al. (1984) found that shear deformation dominated confluence in their model simulation. With respect to the forcing of a warm front, this study found that geostrophic deformation was dominant at low levels, with confluence dominating shear in those cases with the most intense warm fronts. Mudrick (1974) found that confluent geostrophic deformation was favorable for warm frontogenesis, with shear geostrophic deformation favorable for cold frontogenesis.

As mentioned in the last section, confluence dominates shear in Cases 2 and 3, and shear geostrophic deformational forcing dominates confluence at all levels in Case 1. Shear deformation is not as efficient for frontogenesis as confluence and may be a

partial explanation for the lower intensity of the warm front and cyclone in Case 1. The strong frontolytical effect of the surface fluxes in Case 1 to reduce the temperature gradient also prevents the development of a frontal pressure trough. Lack of significant curvature precludes the development of strong confluence. This contrasts with Cases 2 and 3, which develop stronger temperature gradients and more of a pressure trough along the front. In Case 3, which is the first case to develop significant geostrophic deformational forcing, the frontogenetical effect of the friction apparently helps to concentrate the temperature gradient more rapidly in this case. This occurs in spite of relatively strong frontolysis due to surface heating.

2. Frictional Forcing

Baldwin et al. (1984) found that frictional forcing was the dominant forcing at low levels, and Bond and Fleagle (1985) found that frictional convergence in the boundary layer accounted for 90% of the observed total forcing at this level. The results of this study suggest that frictional forcing is not nearly as strong a component of forcing of the warm front, accounting for less than five percent of forcing at low levels. In addition, the pattern of frictional forcing ahead of the warm front is not as consistent in its contribution to forcing of the warm front as it is to the forcing of the cold front found in these other studies. It is not known whether this weaker forcing by friction in the warm front studied here is due to model characteristics or some fundamental difference between warm and cold fronts. The stronger frictional forcing and more intense cold front in Case 3 compared with Case 1 suggest that frictional forcing can greatly enhance frontogenesis. This enhancement is partially due to indirect effects on other more dominant processes.

In addition, frictional forcing of the warm front is not consistently predictable as to whether it is frontogenetical. As shown in the results, sometimes the boundary between the regions of positive and negative forcing was such as to oppose the forcing by the other terms and sometimes it seems to enhance the forcing by the other terms. The development of these boundaries seems to be closely related to the position of the cyclone and warm front with respect to the surface fluxes, but apparently depends on other factors as well. Surface fluxes remain strongly positive behind the cold front, whereas the flux distribution across the warm front is confused by the pocket of downward heat fluxes near the front and the track of the cyclone relative to the SST gradient.

There is the suggestion of a time lag between frictional forcing and its effect on geostrophic deformational forcing, in particular confluent forcing, in Case 3. The initial development of confluent forcing is preceded by 12 hours of steady, positive frictional

forcing ahead of the warm front, and geostrophic forcing develops 6 hours prior to similar forcing in the other two cases, which have little or no frictional forcing. Similarly, the decrease in the rate of growth of the confluent (and shear) forcing is preceded by 12 hours of increasingly negative frictional forcing in this region. The reversal in the frictional forcing may be influenced by the track of the cyclone relative to the SST gradient. During the first 24 hours, the cyclone tracks towards the region of strong positive heat fluxes and the frictional forcing is frontogenetical. When the cyclone begins to move into colder water and away from the influence of the positive heat fluxes, the frictional forcing becomes frontolytical.

3. Diabatic Heating

Baldwin et al. (1984), using a thermally insulated boundary layer in their model, found that boundary layer heat fluxes had a minimal effect on the synoptic-scale secondary circulation. Bond and Fleagle (1985) included boundary layer heat fluxes in their study, yet found similar results, although boundary layer turbulent heat fluxes were found to be frontolytical in the boundary layer. Nuss and Anthes (1987) found that boundary layer heat fluxes influenced the structure only below 850 mb, suggesting that surface heat flux effects are confined to the boundary layer, due to the influence of the inversion layer above the PBL. This study found similar results in that forcing due to diabatic heating is frontolytical and occurs at low levels only. Its magnitude is comparable to that of shear deformational forcing in Case 2 and confluent forcing in Case 1, and in Case 3 it is about half that of shear. Of interest is the presence of negative forcing in the PBL in Case 2 despite the absence of surface heat and moisture fluxes. This suggests that in the absence of differential surface fluxes, there is surface cooling perceived by the model. This may be the way the model handles convective versus non-convective precipitation, or it may be a result of the computation of this term of forcing due to advection.

C. MID AND UPPER LEVELS

1. Geostrophic Deformation

As with studies of cold front forcing, geostrophic deformational forcing of the warm front at mid levels is dominant within the direct circulation cell ahead of the front, and at upper levels it enhances the upper-level transverse component of the secondary circulation. However, the overall values are typically about 25% of the low-level geostrophic forcing. The weakest mid- and upper-level geostrophic forcing is in Case 2, suggesting that mid- and upper-level geostrophic forcing is not as critical to the devel-

opment of the cyclone as it is at low levels, since this case has the deepest cyclone and strongest geostrophic forcing at the surface.

2. Diabatic Heating

Diabatic heating in the form of latent heat release was found to be the dominant forcing mechanism for the vertical component of the secondary circulation, with positive centers located within and slightly ahead of the updraft region and warm front. All three cases develop some mid-level diabatic forcing due to latent heating in the model. The strongest mid-level latent heating developed in Case 1 and it continued to increase until 42 h. This case was the weakest cyclone, which indicates that latent heating and a strong vertical circulation in the warm front are not the only factors for strong cyclogenesis. Case 3 developes a relatively steady-state of latent heating by 24 h, and the strongest vertical motion, however the diabatic forcing was less than Case 1. This is presumably a feature of the cumulus parameterization in the model. Case 2 has the deepest cyclone by 24 h but produced the weakest mid-level diabatic forcing. This lack of latent heating is probably a reflection of the lack of moisture input from the surface in this case. These results suggest that details of the cumulus parameterization and moist processes in the model strongly alter the intensity of the mid-level diabatic forcing of frontogenesis and the secondary circulation. Since the diabatic forcing is dominant at mid and upper levels, the circulation at these levels will be sensitive to model errors in precipitation processes.

VI. CONCLUSIONS

The results of the model simulations confirm the results of previous observational and numerical studies of frontogenesis. They also suggest important interactions between the surface heat and moisture flux distributions, the forcing of the warm front secondary circulation, and cyclogenesis. Geostrophic deformational forcing was dominant, but evolved differently depending upon surface friction and diabatic heating influences.

The presence of frictional forcing enhances the low-level transverse component of the secondary circulation, which in turn enhances the cold conveyor belt. With strong positive heat fluxes in a favorable location, as in Case 3, frictional forcing appears to enhance development of geostrophic deformational forcing at an earlier stage of cyclogenesis, which also enhances the secondary circulation. As the cyclone and geostrophic deformational forcing intensify, the surface forcing due to friction acts only to modify geostrophic forcing. The development of positive frictional forcing in the latter stages of cyclogenesis, as in Case 1, had little effect on the deepening rate, except perhaps to maintain the geostrophic forcing at such a level as to yield the final 4 mb drop before cyclogenesis finally ceased.

The effect of surface heat and moisture fluxes and their distribution on forcing of the secondary circulation and cyclogenesis is more complex, and the results less definitive than with frictional forcing. Surface forcing due to diabatic heating is consistently frontolytical in each case. The fact that it is a strong component of total forcing in the absence of surface heat and moistrure fluxes, as in Case 2, suggests that either the error is large or there are significant boundary layer differences in the model. Early surface relaxation of the frontal temperature gradient as in Case 1 appears to reduce the potential deepening rate of the cyclone, and dominates frictional forcing.

VII. RECOMMENDATIONS

The results suggest areas for further research, including:

Verify the magnitudes of the various forcing terms in an actual case study. Because the model is drier than real oceanic cyclones, forcing due to diabatic heating effects may be different.

Verify the effect of surface fluxes and boundary layer structure on the frictional forcing of the warm front.

Better understand the role of various model parameterizations involved in determining convective versus non-convective release of latent heat. This may help to explain the presence of negative surface diabatic forcing in the absence of surface heat and moisture fluxes.

LIST OF REFERENCES

Anthes, R. A., 1977: A cumulus parameterization scheme utilizing a one-dimensional cloud model. *Mon. Wea. Rev.*, **105**, 270-286.

_____, E.-Y. Hsie and Y.-H. Kuo, 1987: *Description of the Penn State/NCAR Mesoscale Model Version 4 (MM4)*. NCAR Tech. Note, NCAR TN-282 + STR, 66 pp. (National Center for Atmospheric Research, P.O. Box 3000, Boulder, CO 80307.)

Atlas, R., 1987: The role of oceanic fluxes and initial data in the numerical prediction of an intense coastal storm. *Dynam. Atmos. Oceans*, **10**, 359-388.

Baldwin, D., E.-Y. Hsie and R. A. Anthes, 1984: Diagnostic studies of a two-dimensional simulation of frontogenesis in a moist atmosphere. *J. Atmos. Sci.*, **41**, 2686-2700.

Bond, N. A., and R. A. Fleagle, 1985: Structure of a cold front over the ocean. *Quart. J. Roy. Meteor. Soc.*, **111**, 739-759.

Bosart, L. F., 1981: The Presidents' Day snowstorm of 18-19 February 1979: A subsynoptic scale event. *Mon. Wea. Rev.*, **109**, 1542-1566.

_____, and S. C. Lin, 1984: The Presidents' Day snowstorm of 18-19 February 1979. *Mon. Wea. Rev.*, **112**, 2148-2177.

Businger, J. A., and W. J. Shaw, 1984: The response of the marine boundary layer to mesoscale variations in sea surface temperature. *Dynam. Atmos. Oceans*, **8**, 267-281.

Charney, J. G., 1947: The dynamics of long waves in a barochnic westerly current. *J. Meteor.*, **4**, 135-163.

Chen, T.-C., L.-B. Chang and D. J. Perkey, 1983: Numerical study of an AMTEX '75 oceanic cyclone. *Mon. Wea. Rev.*, **111**, 1818-1829.

Danard, M. B., 1986: On the sensitivity of predictions of marine cyclogenesis to convective precipitation and sea temperature. *Atmos.-Ocean*, **24**, 52-72.

_____, and G. E. Ellenton, 1980: Physical influences on East Coast cyclogenesis. *Atmos.-Ocean*, **18**, 65-82.

Eady, E. T., 1949: Long waves and cyclone waves. *Tellus*, **1**, 33-52.

Eliassen, A., 1959: On the formation of fronts in the atmosphere. *The Rossby Memorial Volume*, Rockefeller Institute and Oxford University, 277-287.

_____, 1962: On the vertical circulation in frontal zones. *Geofys. Publ.*, **24**, 147-160.

Emanuel, K. A., 1985: Frontal circulations in the presence of small moist symmetric stability. *J. Atmos. Sci.*, **42**, 1062-1071.

_____, 1988: Observational evidence of slantwise convective adjustment. *Mon. Wea. Rev.*, **116**, 1805-1816.

Fleagle, R. G., and W. A. Nuss, 1985: The distribution of surface fluxes and boundary layer divergence in midlatitude ocean storms. *J. Atmos. Sci.*, **42**, 784-799.

Gidel, L.T., 1978: Simulation of the differences and similarities of warm and cold surface frontogenesis. *J. Geophy. Res.*, **83**, 915-928.

Hoskins, B.J., and I. Draghici, 1977: The forcing of ageostrophic motion according to the semi-geostrophic equations and in an isentropic coordinate model. *J. Atmos. Sci.*, **34**, 1859-1867.

_____, I. Draghici and H. C. Davies, 1978: A new look at the ω - equation. *Quart. J. Roy. Meteor. Soc.*, **104**, 31-38.

Keyser, D., and R. A. Anthes, 1982: The influence of planetary boundary layer physics on frontal structure in the Hoskins-Bretherton horizontal shear model. *J. Atmos. Sci.*, **39**, 1783-1802.

_____, and M. A. Shapiro, 1986: A review of the structure and dynamics of upper-level frontal zones. *Mon. Wea. Rev.*, **114**, 452-499.

Kuo, H.-L., 1974: Further studies of the parameterization of the influence of cumulus convection on large-scale flow. *J. Atmos. Sci.*, **31**, 1232-1240.

Mudrick, S. E., 1974: A numerical study of frontogenesis. *J. Atmos. Sci.*, **31**, 869-892.

Nuss, W. A., 1989: Air-sea interaction influences on the structure and intensification of an idealized marine cyclone. *Mon. Wea. Rev.*, **117**, 351-369.

_____, and R. A. Anthes, 1987: A numerical investigation of low-level processes in rapid cyclogenesis. *Mon. Wea. Rev.*, **115**, 2728-2743.

Petterssen, S., 1956: *Weather Analysis and Forecasting*. Vol. I, *Motion and Motion Systems*. 2nd ed., McGraw-Hill, New York, 428 pp.

Reed, R. J., and M. D. Albright, 1986: A case study of explosive cyclogenesis in the eastern Pacific. *Mon. Wea. Rev.*, **114**, 2297-2319.

Sanders, F., 1986: Frontogenesis and symmetric stability in a major New England snowstorm. *Mon. Wea. Rev.*, **114**, 1847-1862.

_____, and J. R. Gyakum, 1980: Synoptic-dynamic climatology of the "bomb". *Mon. Wea. Rev.*, **108**, 1589-1606.

Sawyer, J. S., 1956: The vertical circulation at meteorological fronts and its relation to frontogenesis. *Proc. Roy. Soc. London.*, **A234**, 346-362.

Thorpe, A. J., 1984: Convective parameterization in a quasi-geostrophic diagnostic model. *J. Atmos. Sci.*, **41**, 691-694.

Uccellini, L. F., D. Keyser, K. F. Brill and C. H. Wash, 1985: The Presidents' Day cyclone of 18-19 February 1979: Influence of upstream trough amplification and associated tropopause folding on rapid cyclogenesis. *Mon. Wea. Rev.*, **113**, 962-988.

_____, R. A. Petersen, K. F. Brill, P. J. Kocin and J. J. Tuccillo, 1987: Synergistic interactions between an upper level jet streak and diabatic processes that influence the development of a low level jet and a secondary coastal cyclone. *Mon. Wea. Rev.*, **115**, 2227-2261.

Williams, R. T., L. C. Chou and C. J. Cornelius, 1981: Effects of condensation and surface motion on the structure of steady-state fronts. *J. Atmos. Sci.*, **38**, 2365-2376.

INITIAL DISTRIBUTION LIST

		No. Copies
1.	Defense Technical Information Center Cameron Station Alexandria, VA 22304-6145	2
2.	Library, Code 0142 Naval Postgraduate School Monterey, CA 93943-5002	2
3.	Commander Naval Oceanography Command Stennis Space Center, MS 39529-5000	1
4.	Commanding Officer Naval Oceanographic Office Stennis Space Center, MS 39522-5001	1
5.	Commanding Officer Naval Oceanographic and Atmospheric Research Laboratory Stennis Space Center, MS 39529-5004	1
6.	Commanding Officer Fleet Numerical Oceanography Center Monterey, CA 93943-5005	1
7.	Chairman (Code 63Rd) Department of Meteorology Naval Postgraduate School Monterey, CA 93943-5000	1
8.	Chairman (Code 68Co) Department of Oceanography Naval Postgraduate School Monterey, CA 93943-5000	1
9.	Professor W. A. Nuss (Code 63NU) Department of Meteorology Naval Postgraduate School Monterey, CA 93943-5000	5
10.	Professor R. T. Williams (Code 63WU) Department of Meteorology Naval Postgraduate School Monterey, CA 93943-5000	2

11. Lieutenant Commander S. A. Davies 2
USCINCPAC Box 13
Camp H. M. Smith, HI 96861

12. Director 1
Naval Oceanographic and Atmospheric
Research Laboratory
Monterey Detachment
Monterey, CA 93943-5006

13. Director Naval Oceanography Division 1
Naval Observatory
34th and Massachusetts Avenue NW
Washington, DC 20390

14. Chairman, Oceanography Department 1
U.S. Naval Academy
Annapolis, MD 21402

15. Chief of Naval Research 1
800 North Quincy Street
Arlington, VA 22217

16. Office of Naval Research (Code 420) 1
Naval Ocean Research and Development
Activity
800 North Quincy Street
Arlington, VA 22217

17. Library Acquisitions 1
National Center for Atmospheric Research
P.O. Box 3000
Boulder, CO 80307-5000

Thesis
D16923 Davies
c.1 A day in the life of a
warm front.